JOURNAL OF PETROLOGY | VOLUME 45 | NUMBER 3 | PAGES 485–506 | 2004 | DOI: 10.1093/petrology/egg091

A Hornblende Basalt from Western Mexico: Water-saturated Phase Relations Constrain a Pressure–Temperature Window of Eruptibility

J. BARCLAY* AND I. S. E. CARMICHAEL

DEPARTMENT OF EARTH AND PLANETARY SCIENCE, UNIVERSITY OF CALIFORNIA, BERKELEY, CA 94720-4767, USA

RECEIVED AUGUST 25, 2001; ACCEPTED JULY 31, 2003

Trachybasalt scoria from a cinder cone near the Mexican volcanic front contain phenocrysts of olivine with chromite inclusions, apatite, augite and hornblende, with microphenocrysts of plagioclase. The water-saturated phase relations reproduce the phenocryst assemblage between 1040°C and 970°C with water contents of between 2·5 and 4·5% (50–150 MPa). The absence of biotite phenocrysts in the scoria places a tight constraint on the pressure–temperature conditions of phenocryst equilibration, as there is only a small zone where biotite does not accompany hornblende in the experiments. Diluting the fluid phase with CO_2 changes the composition of the olivine, indicating that CO_2 was only a minor component of the fluid of the scoria. Hornblende is stable to 1040°C at oxygen fugacities of NNO + 2 (where NNO is the nickel–nickel oxide buffer), but at lower oxygen fugacities, the upper limit is 990°C. There is a progressive increase in crystallinity in experimental runs as both pressure and temperature decrease. Isobaric plots of crystallinity show that the onset of hornblende crystallization involves a reaction relation, and also results in a marked ~15–40 vol. % increase in crystallinity. Ascending hydrous magmas intersecting the cooler crust could be trapped there by the large increase in crystallinity accompanying the isobaric crystallization of hornblende.

KEY WORDS: *crystallization; eruptibility limit; experiments; hornblende trachybasalt; Mexico*

INTRODUCTION

Water has a profound influence not only on the temperature and depth of melting of arc-related magmas (e.g. Kawamoto & Holloway, 1997; Prouteau *et al*., 2001) but also on melt dynamics, influencing such processes as mixing, assimilation and differentiation (e.g. Gaetani *et al*., 1993; Sisson & Grove 1993; Thomas & Tait, 1997; Hort, 1998), and ultimately controls the eruptive behaviour of the magma on the Earth's surface (e.g. Sparks *et al*., 1994; Bower & Woods, 1997). Volcanic arcs associated with subduction, especially beneath a continental plate, are the sites of the most diverse range of magmatism found on Earth, exemplified by variations in composition and eruptive style.

Estimating the water content of subduction-related magmas is therefore a first-order problem in the petrogenesis of volcanic arcs. Estimates have been obtained from the composition of melt either trapped in phenocrysts within lavas or preserved in quenched glasses from submarine eruptions (Anderson, 1974, 1979; Sisson & Layne, 1993), or by using experimental phase equilibria to reproduce the phenocryst assemblage, the phenocryst composition and the phenocryst abundance of a lava (e.g. Rutherford *et al*., 1985; Blatter & Carmichael, 1998, 2001; Moore & Carmichael, 1998). Such studies have unequivocally demonstrated the importance of water in controlling many aspects of subduction-related magmas. Despite this, there are few examples of high-H_2O basalts that are erupted containing primary hydrous phases (the mineralogical evidence for high water content), with extraordinarily few occurrences documented worldwide [Bogoslof, Alaska, Arculus *et al*. (1977); Kick 'em Jenny, Lesser

*Corresponding author. Present address: School of Environmental Sciences, University of East Anglia, Norwich NR4 7TJ, UK. Fax: +44 (0)1603 507719. E-mail: j.barclay@uea.ac.uk

Antilles, Sigurdsson & Shepherd (1974); Cerro la Pilita, Western Mexico, Luhr & Carmichael (1985); Mount Lamington, Papua New Guinea, Arculus *et al.* (1983)]. This is in spite of the almost ubiquitous presence of amphibole in high-H_2O subduction-related magmas as a whole. This would suggest that either (1) high H_2O content magmas are largely confined to more evolved magmas or (2) there is a correlation between high H_2O content and magma eruptibility in mafic magmas.

The detailed experimental investigation of the role of P–T–H_2O on mineral stabilities and crystallinities in hydrous basaltic magmas currently provides the only way to investigate this relationship in detail. The unique information provided on phenocryst assemblage, composition and abundance provides information of relevance not only to the P–T path of the magma but also to its likely rheological evolution, a factor that can directly control the probability of eruption.

Unfortunately, complete experimental studies of hydrous mafic magmas are comparatively rare.

In this paper we explore the conditions (P–T) of water-saturated phase equilibria for one of the rare hornblende-bearing basaltic magmas (the Cerro la Pilita trachybasalt) and also the effect of CO_2–H_2O on the phase assemblages. By plotting the modal abundance of crystals (referred to subsequently as the crystallinity) on the phase diagram we investigate more fully the role that water played in both magma ascent and eruption. In doing so we also attempt to address broader questions relating to magma ascent and the changing crystallinity and rheology that will ultimately control the eruption of hydrous mafic magmas in subduction zones.

The Cerro la Pilita scoria cone and lava flow

Throughout the last 3 Myr, and particularly in the Quaternary, eruptions of basalt (SiO_2 <52%) have been infrequent in the western Mexican volcanic belt, and of the varieties that do occur (Luhr & Carmichael 1981, sample 22E), those that contain hornblende, and thus display mineralogical evidence of the host magma being hydrous, are very rare. The trachybasalt of a small Quaternary cone (Cerro la Pilita) in the southern part of the Michoacán–Guanajuato Volcanic Field, located in the western portion of the Mexican Volcanic Belt, is the one example found to date. It consists of a scoria cone and lava flow pre-dating the historical (1759–1774) basaltic andesites of Volcan Jorullo, Michoacán (Luhr & Carmichael 1985). Scoria of *ne*-normative trachybasalt (Jor 46) are found high on the cinder cone and are conspicuous for their phenocryst assemblage of hornblende without reaction rims, apatite, olivine and augite, with scattered plagioclase microphenocrysts. On the lower slopes of the Cerro la Pilita cone are small blocks of lava (MAS 2003a) that contain phenocrysts of biotite in addition to the phenocryst phases listed above (but with less augite), and hornblende and plagioclase as unambiguous phenocrysts. The lava emitted from the cone is more siliceous than the scoria, and hornblende, without biotite, occurs therein as residual cores to extensive oxide rims.

Trachybasaltic magmas (LeMaitre *et al.*, 1989) are commonly associated with ocean island basalts and intraplate magmatism, but where they do occur in volcanic arcs, hornblende-bearing trachybasalts are comparatively common, accounting for most of the occurrences of hornblende-bearing basalts as a whole. They also tend to be associated with more K-rich shoshonitic magmas, as in the Atenguillo graben of western Mexico (Wallace & Carmichael, 1992), Papua New Guinea (Ruxton, 1966; Arculus *et al.*, 1983), and the Hellenic Arc (Wyers & Barton, 1986; Barton & Wyers, 1991; Pe-Piper & Piper, 1992). The trachybasalt lava from Jorullo is distinctive because of its local association with basaltic andesite and its very high P_2O_5 content (Table 1), a feature it shares with minettes (lavas with phenocrysts of biotite, apatite and olivine) from western Mexico; however, it is less rich in MgO and Ni than the absarokite lavas associated with minettes (Wallace & Carmichael, 1992; Carmichael *et al.*, 1996).

This paper represents the first attempt to explore the conditions of water-saturated phase equilibria for an erupted basaltic magma that clearly contains hornblende as part of its stable mineral assemblage. Although such a composition may not readily be considered to be representative of an 'average' subduction-related mafic magma, it is necessary to elucidate those conditions under which eruption of hornblende-bearing basalt *is* possible in order to understand why such magmas are largely absent at the Earth's surface.

EXPERIMENTAL PROCEDURES

Synthesis experiments were performed using finely powdered samples of Cerro la Pilita basalt [sample Jor 46 of Luhr & Carmichael (1985)]. Experiments were conducted between 40 and 300 MPa using an internally heated pressure vessel (IHPV) with a vertical rapid quench design (Holloway *et al.*, 1992) with modifications as described by Moore & Carmichael (1998). Experiments were designed to explore all the possible variables that could control phase equilibria and were thus conducted in sealed $Ag_{70}Pd_{30}$ capsules both under water-saturated conditions and with the fugacity of water reduced by half in the vapour phase. For concordance with the natural assemblage,

Table 1: Summary of experimental conditions and phases for water-saturated experiments

Sample no.	*P* (MPa)	*T* (°C)	f_{O_2} (log10)	ΔNNO	Duration (h)	$K_D$ol	Phases
Jor46.6	266	1100	−7·5	1·3	50		ol, S
Jor46.2	212	1100	−6·1	2·7	24	0·36	ol, S
Jor46.11	225	1075	−7·0*	2·1	49	0·39	ol, S, Ap
Jor46.20	232	1060	−7·3*	2·0	49	0·28	ol, cpx, S, Ap
Jor46.5	199	1050	−5·8	3·6	48		ol, cpx, S, Ap
Jor46.10	221	1035	−8·4	1·3	48	0·25	ol, cpx, amph, bi, S, Ap
Jor46.8	214	1035†	−7·8	1·9	48		ol, cpx, amph, bi, S, Ap
Jor46.7	207	1025	−7·9*	1·9	48		amph, bi, S, Ap
Jor46.4	223	1000	−7·2	3·0	60		amph, bi, S, Ap
Jor46.27	148	1040	−8·4	1·2‡	48		ol, bi, S, Ap
Jor46.9	154	1025	−7·9*	1·9	48		ol, cpx, amph, bi, S, Ap
Jor46.24	148	1040	−9·1	0·5‡	45		ol, cpx, S, Ap
Jor46.31	121	967	−8·2	2·0	50	0·27	ol, cpx, amph, bi, S, Ap
Jor46.1	102	1100	−8·2	0·6	45		ol, cpx, Ap, S
Jor46.21	104	1020	−8·0†	1·8	48	0·26	ol, cpx, amph, S, Ap
Jor46.25	110	1010	−9·2	0·6‡	48		ol, cpx, S, Ap
Jor46.26	112	1010	−8·2†	1·8	47		ol, cpx, amph, S, Ap
Jor46.32	117	992	−8·3	2·0	40 + 44§		ol, cpx, amph, S, Ap
Jor46.3	94	1000	−7·2	3·0	30		cpx, amph, S, Ap
Jor46.19	69	1000	−8·8	1·4	53	0·24	ol, cpx, S, Ap
Jor46.30	42	1010	−8·9	1·1	52		ol, cpx, plag, S, Ap
Jor46.29	59	988	−8·7	1·7	24 + 56§		ol, cpx, plag, S, Ap
Jor46.46	48	1000	−8·5	1·7	96¶		ol, cpx, plag, amph, S, Ap
Jor46.28	49	1001	−8·5	1·7	47 + 48§		ol, cpx, S, Ap
Jor46.22	48	950†	−9·3*	1·7	49		ol, cpx, amph, bi, plag, S, Ap
Jor46.23	54	975	−8·8*	1·7	49	0·22	ol, cpx, amph, plag, S, Ap

*No sensor used or sensor capsule lost water during experiment. Oxygen fugacity estimated using best-fit equation for IHPV and 0·1% H_2 mixture of Moore *et al.* (1995). The 95% confidence interval is equivalent to 1 log unit f_{O_2}.
†Large temperature gradient between two thermocouples monitoring sample *T*: Jor46.8 1008 and 1035°C; Jor46.22 1000 and 922°C.
‡Experiment has low f_{O_2} as performed after IHPV vessel flooded with 0·3 wt % H_2 mix.
§Initial experimental conditions: 138 MPa, 997°C (Jor46.32); 128 MPa, 1100°C (Jor46.29); 69 MPa, 1135°C (Jor46.28).
¶Run used homogeneous glass from 1 atm experiments (Table 2) as starting material. Gas replenished halfway through run to ensure stability of f_{O_2}.
$K_D$ol was calculated from exchange reaction with FeO in melt calculated using the known f_{O_2} and expression of Kress & Carmichael (1991). Abbreviations for phases: ol, olivine; cpx, augite; amph, amphibole; bi, biotite; plag, plagioclase; S, spinel or ilmenite; Ap, apatite.

experiments were largely conducted at nickel–nickel oxide (NNO) + 2 but a few runs were also performed at oxygen fugacities (f_{O_2}) equivalent to NNO + 0·5 to investigate the effect of f_{O_2} on the composition of the ferromagnesian phases, particularly the stability of hornblende. Individual run conditions and results from these three sets of experiments are summarized in Tables 1–3. Additionally, four atmospheric pressure experiments were performed in a Deltech VT-31-DT gas-mixing furnace by Mo and Carmichael (Table 4, previously unpublished results) at f_{O_2} equivalent to the NNO buffer.

The sample assembly for a run in the IHPV consisted of a melt capsule and an oxygen sensor capsule connected together and hung from Pt wire. Up to 50 mg of powder was sealed into a capsule of $Ag_{70}Pd_{30}$ with sufficient distilled water to achieve H_2O saturation (water-saturated experiments) or with sufficient crystalline oxalic acid dihydrate to achieve $0{\cdot}5H_2O$ and $0{\cdot}5CO_2$ in the vapour phase during the experiments (H_2O–CO_2 saturated experiments). The $Ag_{70}Pd_{30}$ capsules were welded at both ends and samples were carefully weighed before and after each experiment and then weighed again following puncturing and

Table 2: Compositions of experimental samples from H_2O–CO_2 experiments

Sample no.	*P* (MPa)	*T* (°C)	*f*(H_2O) (MPa)	Phase	*n*	Composition	SiO_2	TiO_2	Al_2O_3	FeO^T	MnO	MgO	CaO	Na_2O	K_2O	Total
Jor46.15	184	1025	86·4	gl	5		52·0(4)*	1·43(13)	19·2(1·0)	5·65(13)	0·22	3·00(0·7)	5·8(1·3)	6·19(55)	3·70(31)	97·53
				ol	8	Fo_{79}	38·1(4)	0·00	0·01	19·8(7)	0·28(4)	40·6(8)	0·22(4)	0·02	0·03	99·17
				A, S	1	$ulv_{28}mt_{27}$	0·08	10·30	9·41	47·62	0·32	7·31	—	—	—	93·64
Jor46.16	170	971	77·3	ol	6	Fo_{74}	37·37(12)	—	—	23·4(1·3)	0·34(7)	37·1(1·1)	0·27(9)	—	—	98·96
				cpx	†											
				plag	6	$An_{38}Ab_{52}Or_7$	56·5(2·4)	0·06	25·9(2·1)	1·1(1)	—	—	7·7(2·5)	6·1(9)	1·2(6)	98·52
				A, S	1	$ulv_{54}mt_{38}$	0·34	18·59	3·35	65·22	0·43	4·15	—	—	—	92·76
Jor46.17	150	1000	69·5	ol	9	Fo_{80}	38·5(9)	—	—	18·0(4·5)	0·21	41·9(4·1)	0·20(2)	—	—	99·05
				cpx	12	$Wo_{46}En_{43}Fs_{11}$	49·0(2·5)	1·3(6)	4·0(1·5)	6·6(1·4)	0·12	14·4(1·2)	22·1(3)	0·59(4)	0·10	98·75
				plag	6	$An_{38}An_{55}Or_8$	57·1(5)	—	25·3(4)	1·05(6)	0·06(2)	0·08(1)	7·6(4)	6·5(6)	1·3(9)	98·91
				A, S		ilm	2·94	48·26	1·22	35·99	0·42	6·13	—	—	—	95·10

n, number of analyses; —, element not analysed or below limit of detection on electron microprobe for particular phenocryst phase.
*One standard deviation of replicate analyses in terms of least units cited.
†Phase not analysed.

Table 3: Experimental compositions from water-saturated experiments on Jor46 performed at oxygen fugacities equivalent to NNO + 0·5

Sample no.	*P* (MPa)	*T* (°C)	Phase σn	*n*	Composition*	SiO_2	TiO_2	Al_2O_3	FeO^T	MnO	MgO	CaO	Na_2O	K_2O	NiO/SrO†	Total
Jor46.42	210	1050	gl	7		48·85(20)	1·31(31)	15·05(19)	6·4(4)	0·08(7)	3·90(3)	6·53(14)	4·72(16)	3·16(4)		89·97
			ol	7	$Fo_{82·3}$(6)	39·46(30)	—(6)	—	16·2(5)	0·24(3)	43·7(5)	0·23(3)	—	—	0·26(6)	100·23
			cpx	7	$Wo_{46·2}(5)En_{45·5}(6)Fs_{8·5}(1·8)$	52·4(1·1)	0·70	1·88(28)	5·4(8)	—	16·16(3)	22·9(8)	0·35(18)	—	—	100·22
			F‡	1		0·35	1·85	11·79	34·37	0·25	7·94	0·27	38·98	0·15	0·25	96·257
Jor46.44	200	980	gl	1		56·0	0·79	17·00	4·28	0·06	1·29	2·75	6·21	3·72		92·18
			ol	7		38·6(1·2)	—	—	18·9(4·7)	0·27(10)	41·3(4·3)	0·24(4)	—	—	—	99·49
			cpx	1		52·68	0·57	1·53	5·18	0·09	16·29	22·47	0·36	0·06		99·24
			amph	9		41·6(3)	2·6(3)	11·1(4)	11·4(9)	0·15(5)	14·4(1·0)	11·0(4)	2·81(11)	0·95(8)	0·19(5)	96·01
			F	1		0·18	10·17	3·57	75·18	0·33	2·86	0·09	—	—		92·57
Jor46.40	159	997	gl	1		49·58	1·43	15·65	6·30	0·11	3·25	5·79	5·08	3·21		90·40
			ol	8	$Fo_{80·7}$(4)	39·01(26)	—	—	17·9(4)	0·26(4)	41·9(3)	0·29(2)	—	—	0·16	99·73
			cpx		$Wo_{47·5}(3)En_{42·3}(2)Fs_{10·2}(4)$	50·3(5)	1·29(18)	3·4(4)	6·38(23)	0·11(4)	14·81(10)	23·11(20)	0·41(4)	—	—	100·23
			F	1		0·15	3·39	7·24	44·41	0·32	6·53	0·08	32·61	0·13	0·11	95·00
Jor46.41	155	970	gl			53·5(3)	0·71(6)	16·54(19)	5·22(20)	0·09(3)	2·00(3)	4·19(7)	5·86(11)	3·46(8)	—	91·59
			ol cores		$Fo_{78·8}$(2·4)	39·1(4)	—	—	20·0(2·1)	0·32(4)	40·7(1·8)	0·21(4)	—	—	0·21	100·65
			cpx													
			amph	1		41·03	3·03	11·27	10·92	0·11	14·30	11·81	2·51	0·98	0·21	96·60
			bi			38·80	3·13	13·80	9·60	0·05	19·32	0·20	1·10	8·33	0·71	95·80
			F	5		0·11	2·87	5·84	51·21	0·44	4·58	0·16	27·72	0·15	0·09	93·21
Jor46.33	150	999	gl	—												
			ol		Fo_{81}(1)	39·25(29)	—	—	17·4(1·2)	0·26(6)	42·9(1·1)	0·20(5)			0·3(1)	100·40
			cpx		$Wo_{47·0}(0·5)En_{43}(3)Fs_{10}(2)$	51·0(1·7)	1·1(5)	2·9(1·4)	6·48(1·2)	0·12(2)	15·3(1·2)	22·86(18)	0·46(7)	—	—	100·42
			F			0·19	8·21	4·92	65·75	0·31	5·73	0·15	7·64	0·38	0·31	93·61
Jor46.24	148	1040	gl	—												
			ol	7	$Fo_{82·9}$(5)	39·00(25)			16·0(5)	0·27(6)	43·51(24)	0·22(2)	—	—	—	99·1
			cpx	8	$Wo_{46}(1)En_{43}(1)Fs_{11}(1)$	49·8(1·1)	1·13(28)	3·3(8)	7·0(6)	0·15(6)	14·9(7)	22·1(3)	0·55(10)			99·09
			F			0·12	6·99	5·1	7·91	65·93	0·41	6·29	—	—	—	92·96

Table 3: continued

Sample no.	*P* (MPa)	*T* (°C)	Phase σn	*n*	Composition*	SiO_2	TiO_2	Al_2O_3	FeO^T	MnO	MgO	CaO	Na_2O	K_2O	NiO/SrO†	Total
Jor46.25	110	1010	gl	—												
			ol	—												
			cpx		$Wo_{46}(1)En_{45}(2)Fs_9(1)$	51·7(8)	0·69(18)	2·2(6)	5·6(6)	0·10(3)	16·0(7)	22·5(5)	0·45(6)	—	—	99·63
			F			0·13	4·18	5·38	15·26	59·91	0·29	—	7·05		0·12	92·86
Jor46.1	102	1100	gl													
			ol	10	$Fo_{87}(1)$	39·89(28)	—	—	12·8(1·0)	0·24(5)	46·2(9)	—	0·22(4)	—	—	99·08
			cpx	5	$Wo_{46}(2)En_{44}(1)Fs_{10}(2)$	49·9(1·5)	1·02(17)	3·3(9)	6·3(6)	0·10(3)	15·2(5)	22·60(9)	0·46(4)	—	—	99·39
			F			0·08	3·35	4·45	7·64	66·83	0·22	7·7	0·68	—	—	90·94
Jor46.35	59	1075	gl													
			ol	6	$Fo_{83·0}(0·5)$	39·64(25)	—	—	16·0(4)	0·22(4)	43·94(29)	0·24(9)	—	—	0·24(9)	100·32
			cpx		$Wo_{46}(1)En_{45}(1)Fs_9(1)$	51·8(1·1)	0·73(29)	2·3(7)	5·6(6)	0·13(2)	15·9(7)	22·9(5)	0·42(6)	—	—	100·14
			F			0·15	4·97	7·58	52·10	0·29	7·96	0·20	19·75	0·28	0·36	93·66

Mineral abbreviations as in Table 1, except F (Fe–Ti oxide). *n*, number of analyses. Where multiple analyses were made the number in parentheses is 1σ of all analyses cited in least units of average. —, element not analysed or below limits of detection for operating conditions of electron microprobe.
*Mineral formula calculated using mol %.
†NiO cited for ol, cpx, F and SrO cited for amph, and BaO for analysis of biotite in Jor46.41.
‡For iron–titanium oxides Na_2O and K_2O columns represent oxide wt % of Cr_2O_3 and V_2O_3, respectively.

Table 4: Run conditions and phases for 10^5 Pa NNO phase equilibria experiments

Sample no.	T (°C)	Phase*	Mode (%)	Composition	SiO_2	TiO_2	Al_2O_3	FeO	MgO	CaO	Na_2O	K_2O	P_2O_5	Cr_2O_3	Total
Jor46.1atm.5	1250	gl(6)			49·28(52)†	1·25(16)	13·78(21)	7·94(30)	8·37(11)	7·77(12)	4·44(15)	2·64(7)	1·24(13)		97·41
Jor46.1atm.6	1225	gl(7)	97		50·48(38)	1·47(37)	14·30(12)	7·51(46)	7·48(15)	8·12(32)	4·58(20)	2·77(9)	1·21(25)		98·75
		ol(9)	3	$Fo_{88·1}$(5)	40·14(19)			11·5(5)	47·4(4)	0·17(2)					99·76
Jor46.1atm.7	1200	gl(5)	94		50·55(11)	1·36(20)	14·53(15)	7·19(37)	6·45(12)	8·03(20)	4·60(15)	2·83(16)	1·04(8)		97·14
		ol(8)	4	$Fo_{86·3}$(3)	39·77(41)			13·01(33)	45·9(4)	0·40(5)					99·73
		sp(2)			0·14	1·79	14·83	26·06	0·21					41·15	
Jor46.1atm.8	1185	gl(3)	92		50·86(13)	1·30(46)	15·02(15)	6·58(27)	5·84(13)	8·52(37)	4·33(12)	2·74(9)	1·05(3)		96·94
		ol(7)	6	$Fo_{85·8}$(2)	39·84(23)			13·43(22)	45·7(5)	0·44(14)					100·00
		sp(2)			0·14	2·18	15·36	24·35	12·25					39·98	
Jor46.1atm.9	1175	gl(3)	93		50·48(26)	1·47(10)	14·83(22)	7·68(30)	5·44(9)	8·56(7)	4·82(14)	2·83(19)	1·40(8)		98·25
		ol(6)	7	$Fo_{84·2}$(2)	39·59(23)			14·84(16)	44·47(34)	0·43(4)					99·79
		sp‡	1												

*Number in parentheses denotes number of analyses.
†One standard deviation of replicate analyses in terms of least units cited.
‡Fe–Ti oxides in 1atm.9 were too small to analyse.

drying ($\sim$100°C) for 5 min to confirm the presence of a fluid phase at the end of the run. This alloy has been consistently shown to minimize iron loss in H_2O-rich experiments (Sisson & Grove, 1993; Grove *et al.*, 1997; Blatter & Carmichael, 1998; Moore & Carmichael, 1998) and our analysis of capsule material after the runs confirms that iron loss to the capsule was below the limit of detection (500 ppm). Pressure was measured with a calibrated Heise gauge accurate to $\pm$5 bars and temperature was monitored using three (one opposite the melt, one at the bottom of the melt capsule, one opposite the base of the sensor capsule) 'K' type thermocouples calibrated to $\pm$5°C of the melting point of gold. The temperature gradient was generally less than 10°C across the melt capsule; if the gradient was greater, then this is noted in Table 1. The f_{O_2} was buffered at approximately NNO + 2 by using 0·1 vol. % H_2 in the argon pressurizing medium, and monitored using a H_2O-saturated, compressed 50–50 mol % Ni–Pd pellet, isolated from the $Ag_{70}Pd_{30}$ capsule within an alumina sleeve. The f_{O_2} values were calculated based on the mole fraction of Ni in the sensor capsule corrected for any differences in melt and sensor temperature (usually $T_{melt} \pm 30$°C) using the calibration of Pownceby & O'Neill (1994). The estimated error on reported f_{O_2} values as the result of uncertainty in temperature, inhomogeneity of Ni–Pd powder, and analytical error is $\pm$0·2 $\log_{10}$ units f_{O_2}.

ANALYTICAL TECHNIQUES

Experimental glasses and minerals were analysed on the Cameca SX-50 microprobe at UC Berkeley. All mineral phases were analysed using an accelerating voltage of 15 kV, and a beam current of 20 nA. A focused beam was used for olivine, augite, oxides and apatite, and a slightly defocused beam (5 μm) was used for biotite, hornblende and plagioclase, to minimize alkali loss. Standards used were oxides of Mg, Si, Al, Ti, Mn, V, Cr, synthetic fayalite (Fe), diopside (Ca), nepheline (Na), orthoclase (K), strontium titanate (Sr), fluor-phlogopite (F) and chlor-apatite (Cl and P). MAN corrections (Donovan & Tingle, 1996) and 10 s counting times were used on major elements (Si, Al, Mg, Fe, Ca, Na, K). Longer count times and off-peak corrections were applied to less abundant elements (Ti, Mn, Sr, P, Cl, F) as appropriate. A natural kaersutite sample, analysed by wet chemistry (Brown & Carmichael, 1969), was used as an internal secondary standard throughout each analytical session. Tabulated analyses are the result of multiple analyses of rims and cores of several different crystals unless otherwise stated.

The Ni–Pd alloy compositions of the oxygen sensors were analysed using a focused beam and a sample current of 40 nA. The reported alloy compositions are the average of 5–10 individual grain analyses, with $1\sigma < 3$ mol % Ni.

Hydrous glasses were analysed using a 5 nA, 20 μm beam to minimize sodium loss. A less defocused beam and a slightly stronger beam current using an on-line Volatile Element Correction procedure (where Na, K and Si counts were monitored every 2 s) was also used, and it was shown that although the precision of these measurements was greater, the former method gave preferred results. As the result of volatile element loss, we estimate the error in Na is ~10%. Using such a broad beam presented some difficulties in analysing melt pools in crystal-rich experiments. However, with the large sample sizes, this was possible in all but a few of the 50 MPa experiments. In some cases, only single analyses are presented as the number of melt pools >20 μm was limited. The analytical totals of the hydrous glasses are systematically low (Table 5).

Modal calculations

Mineral modes were calculated using a least-squares model (XTALFRAC, Stormer & Nicholls, 1981), assuming that the initial bulk composition of Jor 46 remained constant, which therefore represented the sum of the crystalline phases and the quenched glass. Although more practicable and accurate than point counting, this method is affected by the uncertainty in the analyses of the experimental glass and phenocryst phases. This is evident in the more crystalline experimental samples where the largest array of phenocryst phases are present, most of which have some degree of compositional zoning. To illustrate this, we compared least-squares calculations where we used: (1) the average crystal compositions; (2) average composition $\pm 1\sigma$ for each of the experimental runs. This produced a maximum variation of 10% in the total crystallinity (much less for samples with <20 wt % crystals), although the relative uncertainty for individual phenocryst modes varied between 0 and 25%. We regard our estimates of crystallinity to have a maximum uncertainty of ±10% but we found that the relative error associated with the abundance of individual phases can be greater, especially for the less abundant phenocryst phases. The calculated modes are given in Table 5.

Mineral nomenclature

The synthesized and natural calcic amphibole has nearly fully occupied A-sites and can be classified as pargasite (Leake *et al.*, 1997). However, in keeping with earlier studies of amphibole stability in basaltic magmas (Helz, 1973; Sisson & Grove, 1993), and lacking Fe^{3+} determinations, this amphibole is more simply described as hornblende. Following Luhr & Carmichael (1985), we refer to the high Ca-pyroxene synthesized in the experiments as augite. Although a range of iron–titanium oxides (chrome spinel to titanomagnetite) has been synthesized, depending on the P, T and f_{O_2}, we refer to the accessory oxide phase as spinel. Using the mica classification of Deer *et al.* (1997), whereby molar $Mg:Fe_{total} < 2:1$, the synthesized mica is referred to as biotite.

RESULTS

Attainment of equilibrium

The majority of experiments in this study are direct synthesis runs in which crystals have grown from melt. Where sufficient melt pools are available to make multiple analyses, the experimental glasses are homogeneous in composition (Table 5), with synthesized crystals generally being euhedral and equant or tabular, and in the less crystalline experiments they tend to reach sizes of >100 μm (see Fig. 5, below). In general, we note that runs with <15 wt % crystals tend to have very homogeneous crystal populations, and our calculated mineral–liquid partition coefficients (Table 1) for olivine and glass are similar to those reported by Sisson & Grove (1993); however, some zonation is inevitable in more densely crystalline experiments, and an increase in both inter- and intra-grain compositional variation is observed, as also noted by Sisson & Grove (1993) and Moore & Carmichael (1998).

To test equilibrium in these cases, we ran three experiments where the T or P was initially held at higher values, followed by ~48 h at the recorded run conditions (Table 1; Jor46.32, Jor46.29 and Jor46.28). We noted no difference between either the phenocryst assemblage or their compositions within these experiments (Tables 6–11) and the direct synthesis experiments, although some olivine cores within the ~50 MPa experiments are clearly relict from the initial higher T conditions. However, to test this further, we also conducted one experiment at 48 MPa and 1000°C (Jor46.46) using a homogeneous glass from the 10^5 Pa experiments. Here, although hornblende was stable, no plagioclase was found to be present, conflicting slightly with the findings for Jor46.28. Both these experiments are very close to the stability limit of both plagioclase and hornblende, reflecting the difficulty of plagioclase nucleation when using glassy starting materials (Weber & Pichavant, 1986). Phase compositions are otherwise similar and this discrepancy was observed only in these crystal-rich experiments. A few relict grains were detected in the experiments, other than the presence of occasional chromite cores ($\ll$1 vol. %) within some spinels, which may have originated from inclusions within the natural olivines. Although equilibrium cannot be unequivocally

Table 5: Electron microprobe analyses and calculated normative compositions of experimental glasses

Sample no.:	Jor46*	Jor46.2	Jor46.11	Jor46.20	Jor46.10	Jor46.4	Jor46.31	Jor46.21	Jor46.3	Jor46.19	Jor46.23
P (MPa):		212	225	232	221	223	121	104	94	69	54
T (°C):		1100	1075	1060	1035	1000	967	1020	1000	1000	975
Wt % xls		7·3	9·6	14·9	31	41	45	48	52	23	60
ol		5·6	8·0	7·2	—	—		6	—	17	1
cpx		—	—	5·9	5·6	—		—†	—	—†	—†
hbl		—	—	—	18·3	33·2		35	46	—	48
bi		—	—	—	5·1	2·5		—	—	—	—
S + Ap		1·7	1·6	1·8	1·8	5·3		7	6	6	11
n		6	6	6	3	6	3	1	9	9	1
SiO_2	49·21	46·64(18)	48·02 (42)	50·08(73)	52·01(49)	53·1(9)	57·08(20)	56·34	56·69(59)	53·3(1·3)	60·54
TiO_2	1·33	1·47(18)	1·71(17)	1·51(22)	0·94(22)	0·49(19)	0·42(10)	0·79	0·38(10)	1·5(3)	0·55
Al_2O_3	14·19	13·76(30)	14·22(9)	15·07(6)	16·01(21)	15·61(20)	15·96(14)	17·37	16·85(23)	16·81(27)	18·22
Fe_2O_3‡		3·75	3·30	3·23	2·18	1·92	1·90	1·86	2·59	2·62	1·00
FeO		3·28	3·65	3·87	3·64	1·51	1·78	2·35	2·07	4·10	1·26
MnO	0·12	0·12(4)	0·10(8)	0·09(8)	0·13(9)	0·09(5)	0·05	0·10	0·09(4)	0·13(9)	0·05
MgO	8·32	5·45(8)	4·80(14)	4·46(12)	2·90(5)	2·70(10)	1·45(9)	1·95	1·56(17)	3·34(12)	0·92
CaO	7·68	7·5811)	7·68(20)	6·78(22)	4·80(10)	3·80(9)	2·70(6)	3·44	2·25(31)	6·13(29)	2·03
Na_2O	4·59	4·25(3)	4·52(20)	4·70(14)	5·51(10)	4·6721)	5·65(31)	5·71	5·56(23)	5·4(4)	6·62
K_2O	2·82	2·80(5)	2·92(8)	3·10(15)	3·20(5)	3·35(12)	3·98(6)	4·08	4·29(13)	3·4(11)	4·50
H_2O§	1·19	5·26	5·53	5·66	5·36	5·55	4·13	3·51	3·43	3·0	2·53
Total		94·36	96·45	98·55	96·68	92·79	94·10	97·50	95·76	99·73	98·22
Qz¶	—	—		—	—	1·27	1·18	—	1·43		—
Co	—	—		—	—	—	—	—	—		—
Or	16·65	16·53	17·24	18·30	18·89	20·25	23·40	24·08	25·32		26·56
Ab	27·34	24·78	23·85	28·95	37·90	39·14	47·76	45·98	47·00		55·59
An	9·74	10·20	9·89	10·87	9·51	12·66	6·44	9·72	8·36		6·72
Lc	—	—	—	—	—	—	—	—	—		—
Ne	6·21	6·04	8·05	5·84	4·70	—	—	1·24	2·18		0·20
Di	19·19	21·37	22·32	18·06	11·59	4·89	5·73	5·95	2·86		2·74
Hy	—	—	—	—	—	5·03	3·92	—	—		—
Ac	—	—	—	—	—	—	—	—	—		—
Ol	10·47	2·59	2·32	3·28	3·80	—	—	3·24	3·07		1·81
Mt	6·60	5·46	4·55	4·75	3·18	2·79	1·57	2·22	0·72		0·96
Ilm	2·53	2·80	3·25	2·87	1·79	1·14	0·80	1·50	1·45		1·05
Hm	—	0·27	—	—	—	—	—	—	—		—

*Wet chemical analysis by I. S. E. Carmichael & J. Hampel from Luhr & Carmichael (1985).
†Cpx used in calculation as reactant.
‡Ratio of FeO to Fe_2O_3 calculated using method of Kress & Carmichael (1991) for measured f_{O_2} and glass composition.
§H_2O solubility calculated for each glass composition at relevant pressure and temperature using the model of Moore *et al.* (1998).
¶Norm calculated using *Magma* v2.3 authored by Ken Wohletz.
Wt % xls, amount of crystals in experimental charge calculated by mass balance using glass and phenocryst compositions using least-squares model of Stormer & Nicholls (1981). Abbreviations are as for Table 1. *n*, number of analyses; where melt pool is restricted 'best' analysis is quoted rather than average composition (see analytical techniques section for discussion). Values in parentheses represent 1σ variation of analysed glasses, shown in terms of least units cited.

demonstrated in all experimental samples, we nevertheless believe that a close approach to equilibrium has been attained, sufficient to interpret several aspects of the evolution of the Cerro la Pilita magma.

Water-saturated phase equilibria

The phase stability fields for the trachybasalt have been determined for P_{H_2O} up to 300 MPa and are plotted in Fig. 1 for experiments equilibrated at

Table 6: Experimental and natural olivine compositions

Sample:	Jor46[1]	Jor46[1]	MAS 2003a	Jor46.6	Jor46.11	Jor46.20	Jor46.2	Jor46.5	Jor46.10	Jor46.8	Jor46.9	Jor46.27	Jor46.24	Jor46.31	Jor46.32
P (MPa):	rim	core		266	225	232	212	199	221	214	154	148	126	121	117
T (°C):				1100	1075	1060	1100	1050	1035	1035	1025	1040	1040	967	992
n:			7	7	5	6	8	10	6	7	7	5	7	4	4
SiO_2[2]	38·74	39·17	40·16	40·2(3)	39·74(21)	39·4(7)	39·8(4)	40·1(3)	39·6(4)	39·2(3)	39·2(4)	40·1(2)	39·00(25)	39·34(14)	39·23(23)
FeO*	13·88	11·89	12·56	11·4(6)	13·54(25)	12·0(6)	10·6(1·2)	12·11(30)	14·0(1·7)	16·4(1·2)	15·8(8)	12·2(3)	16·0(5)	14·7(1·1)	14·9(4)
MnO	0·19	0·10	0·16	0·20(4)	0·21(2)	0·21(2)	0·18(5)	0·24(2)	0·23(13)	0·27(7)	0·27(7)	0·19(4)	0·27(6)	0·30(3)	0·27(2)
MgO	47·08	48·67	47·07	47·3(6)	45·61(23)	48·32(24)	48·8(6)	46·7(6)	45·1(1·4)	43·6(1·0)	43·2(6)	46·8(3)	43·51(24)	44·7(8)	44·85(17)
NiO	—	—	—	—	0·50(6)	—	—	—	—	—	—	0·42(5)	—	0·47(26)	0·25(6)
CaO	0·12	0·12	0·13	0·21(2)	0·25(5)	0·22(6)	0·20(4)	0·18(3)	0·20(5)	0·17(2)	0·19(1)	0·24(2)	0·22(2)	0·15(2)	0·20(1)
Total	100·03	99·56	100·08	99·39	100·07	100·29	99·59	99·49	99·70	100·12	98·74	100·02	99·10	99·76	99·83
Mol % Fo	85·8	87·8	87·0	88·1(7)	85·7 (3)	87·8(5)	89·2(1·2)	87·3(4)	85·1(1·9)	82·5(1·4)	83·0(9)	87·3(2)	82·9(5)	84·4(1·2)	84·3(4)
Fa	14·2	12·2	13·0	11·9(7)	14·3(3)	12·2(5)	10·8(1·2)	12·7(4)	14·9(1·9)	17·5(1·4)	17·0(9)	12·7(2)	17·1(5)	15·6(1·2)	15·7(4)

Sample:	Jor46.26	Jor46.1	Jor46.21.	Jor46.19	Jor46.29	Jor46.23	Jor46.28	Jor46.22	Jor46.30
P (MPa):	112	102	104	69	59	54	49	48	42
T (°C):	1010	1100	1020	1000	988	975	1001	1000	1010
n:	8	10	6	8	4	8	5	5	6
SiO_2	39·36(17)	39·89(28)	39·20(32)	40·0(4)	38·8(3)	39·73(32)	38·1(5)	39·86(31)	39·82(12)
FeO*	14·95(39)	12·8(1·0)	14·0(8)	17·5(4)	18·8(2·1)	13·5(1·1)	21·3(3·4)	12·5(9)	12·9(7)
MnO	0·25(5)	0·24(5)	0·31(5)	0·25(3)	0·27(9)	0·28(9)	0·33(10)	0·21(6)	0·24(6)
MgO	44·4(6)	46·2(9)	45·3(4)	46·3(0·6)	41·3(1·6)	45·3(1·0)	39·3(3·3)	46·3(8)	46·4(6)
NiO	0·26(8)	—	—	—	0·34(5)	—	0·29(9)	—	—
CaO	0·21(5)	0·22(4)	0·20(1)	0·20(3)	0·19(4)	0·22(4)	0·25(6)	0·18(4)	0·18(2)
Total	99·62	99·08	99·20	100·30	79·6(2·4)	99·34	99·80	99·22	99·87
Fo	84·1(5)	86·6(1·1)	85·2(8)	85·9(5)	79·6(2·4)	85·6(1·2)	76·5(4·2)	86·8(1·0)	86·5(7)
Fa	15·9(5)	13·4(1·1)	14·8(8)	14·1(5)	20·4(2·4)	14·4(1·2)	23·5(4·2)	13·2(1·0)	13·5(7)

[1] Representative analyses of olivine in Jor46 scoria.
[2] Analysis cited with 1σ from multiple analyses (1σ in term of least units cited).
n, number of analyses; FeO*, total iron expressed as FeO.

Table 7: Natural and experimental hornblende compositions

Sample:	Jor46*	MAS 2003a	Jor46.4	Jor46.10	Jor46.8	Jor46.7	Jor46.9	Jor46.31	Jor46.32	Jor46.26	Jor46.21	Jor46.3	Jor46.23	Jor 46.46	Jor46.22	Jor46.30	Jor46.41†	Jor46.44
P (MPa):	—		223	221	214	207	154	121	117	112	104	94	54	48	48	42	155	200
T (°C):	—		1000	1035	1035	1025	1025	967	992	1010	1020	1000	975	1000	950	1010	970	980
n:		12	10	5	5	6	4	8	8	5	8	8	5	9	10	3	3	3
SiO_2	41·65	42·00	42·1(8)	41·8(4)	42·5(6)	41·9(6)	41·5(3)	41·7(8)	41·2(6)	40·5(18)	41·2(4)	41·4(4)	41·7(3)	41·2(5)	41·0	40·8(5)	41·03	41·6(3)
TiO_2	3·18	3·00	2·4(4)	2·7(2)	2·2(0·2)	2·6(4)	2·8(6)	2·9(6)	3·1(5)	3·7(3)	3·2(3)	3·3(6)	3·2(12)	4·1(4)	3·95(26)	3·7(7)	3·03	3·7(7)
Al_2O_3	11·47	11·05	10·7(3)	11·0(4)	10·5(3)	11·1(5)	10·9(4)	11·3(6)	11·2(3)	11·7(3)	11·3(3)	10·9(2)	11·1(2)	11·4(4)	11·5(4)	11·2(4)	11·29	11·1(4)
FeO	9·44	9·77	8·6(9)	9·1(3)	9·7(3)	10·4(9)	9·8(4)	9·5(3)	9·6(2)	9·0(3)	9·1(5)	9·4(5)	9·4(4)	9·1(4)	8·7(2)	9·4(4)	10·92	11·4(9)
MnO	0·07	0·10	0·11(4)	0·07(2)	0·12(3)	0·13(3)	0·13(4)	0·12(5)	0·10(3)	0·09	0·10(4)	0·12(4)	0·12(3)	0·12(3)	0·12(3)	0·09(1)	0·11	0·15(5)
MgO	15·44	15·53	17·0(9)	16·0(2)	15·9(5)	14·8(9)	15·4(2)	15·5(5)	15·5(4)	15·2(2)	15·5(3)	15·9(4)	15·4(3)	15·3(6)	15·6(5)	15·37(27)	14·3	14·4 (1·0)
CaO	11·88	11·76	11·7(2)	11·7(1)	11·4(4)	11·5(1)	11·5(1)	11·5(3)	11·77(10)	12·1(4)	11·6(2)	11·77(12)	11·6(2)	11·37(25)	11·56(21)	11·68(16)	11·81	11·0(4)
Na_2O	2·71	2·71	2·68(8)	2·64(3)	2·75(5)	2·8(1)	2·7(1)	2·78(13)	2·68(5)	2·55(8)	2·71(5)	2·66(6)	2·75(13)	2·84(11)	2·84(8)	2·68(11)	2·51	22·84(11)
K_2O	0·26	1·08	0·93(9)	1·03(4)	1·00(1)	0·8(2)	1·00(1)	0·99(15)	1·12(11)	1·09(5)	1·06(7)	1·12(12)	1·05(10)	0·92(13)	0·91(5)	1·08(6)	0·98	0·95(8)
Total	97·71	97·41‡	96·10	96·50	96·58	96·51	96·34	96·80	96·92	96·59	95·85	96·54	96·80	96·30	96·24	96·82	96·24	95·06
Si^{4+}†	—	—	6·77	6·75	6·84	—	—	6·76	—	—	6·67	6·69	6·75	6·62	—	—	6·75	6·85
Ti^{4+}	—	—	0·29	0·33	0·27	—	—	0·35	—	—	0·39	0·40	0·39	0·50	—	—	0·37	0·32
Al^{3+}	—	—	1·01	1·05	1·04	—	—	1·08	—	—	1·08	1·04	1·04	1·08	—	—	1·09	1·08
Fe^{3+}	—	—	0·31	0·21	0·28	—	—	0·31	—	—	0·27	0·34	0·31	0·25	—	—	0·26	0·27
Fe^{2+}	—	—	0·54	0·80	0·75	—	—	0·66	—	—	0·69	0·58	0·66	0·86	—	—	0·86	0·85
Mn^{2+}	—	—	0·01	0·01	0·02	—	—	0·02	—	—	0·01	0·02	0·01	0·02	—	—	0·01	0·02
Mg^{2+}	—	—	4·07	3·85	3·81	—	—	3·74	—	—	3·84	3·83	3·72	3·67	—	—	3·51	3·54
Ca^{2+}	—	—	2·02	2·03	1·97	—	—	2·00	—	—	2·04	2·04	2·01	1·96	—	—	2·08	1·94
Na^{+}	—	—	0·42	0·41	0·43	—	—	0·42	—	—	0·42	0·42	0·43	0·44	—	—	0·40	0·45
K^{+}	—	—	0·10	0·11	0·10	—	—	0·10	—	—	0·12	0·12	0·11	0·09	—	—	0·10	0·09
Total	—	—	15·54	15·55	15·51	—	—	15·44	—	—	15·53	15·48	15·43	15·49	—	—	15·43	15·41

*Analysis taken from Luhr & Carmichael (1985).
†Hornblende formula calculated using ratio of Fe_2O_3/FeO in melt calculated from microprobe analysis of glass using Kress & Carmichael (1991). Where no glass is available, formula is not calculated. Jor46.41 and Jor46.44 are hornblendes from experiments run at oxygen fugacities equal to NNO + 0·5.
‡Includes 0·03 Cr_2O_3, 0·09 BaO, 0·29 F.

Table 8: Experimental and natural spinel compositions

Sample:	Jor46*	Jor46*	Jor46.6	Jor46.11	Jor46.20	Jor46.4	Jor46.2	Jor46.5	Jor46.8	Jor46.10	Jor46.7	Jor46.9	Jor46.24	Jor46.31
P (MPa):	(a)	(b)	266	225	232	223	212	199	214	221	207	154	126	121
T (°C):	—	—	1100	1075	1060	1000	1100	1050	1035	1035	1025	1025	1040	967
SiO_2	0·07	0·17	0·14	0·17	0·14	0·09	0·09	0·08	0·29	0·15	0·07	0·20	0·12	0·13
TiO_2	1·57	8·11	2·61	2·92	3·62	1·99	1·98	3·71	5·39	5·71	3·27	4·91	6·99	3·52
Al_2O_3	10·60	3·22	5·47	6·81	3·91	3·99	4·00	3·60	3·28	3·81	3·27	3·41	5·10	3·16
Cr_2O_3	40·97	0·22	15·72	26·17	4·30	5·03	4·55	1·15	0·76	1·24	0·00	0·05	7·91	0·09
FeO	33·14	75·60	57·80	46·46	72·46	70·21	70·16	74·97	76·77	74·80	77·81	77·49	65·93	80·64
MnO	0·26	0·48	0·25	0·25	0·24	0·16	0·16	0·21	0·32	0·29	0·38	0·30	0·41	0·36
MgO	10·47	6·59	8·99	8·24	7·14	8·67	8·68	7·01	4·07	5·28	5·18	4·37	6·29	3·94
NiO	0·06	0·05	0·51	0·52	—	0·71	0·71	0·31	0·18	0·35	0·24	0·08	—	—
V_2O_3	0·30	0·14	—	—	0·0	—	—	—	—	—	—	—	—	0·14
Total	97·46	94·66	91·49	91·52	91·89	90·85	90·32	91·04	91·06	91·62	90·21	90·78	92·96	92·14
Fe_2O_3	16·44	52·25	43·17	28·95	55·90	57·44	57·59	57·80	52·95	51·10	58·76	54·77	42·50	58·70
FeO	18·34	28·58	18·95	20·41	22·91	18·53	18·34	22·96	29·12	28·6	24·94	28·20	27·69	27·82
Total	99·10	99·89	95·81	94·45	97·82	96·61	96·09	96·83	96·37	94·4	96·10	96·27	97·00	97·97
Cr no.	72	4	66	72	60	15	43	18	13	18	00	1	51	2
Mg no.	50	29	46	47	23	46	46	35	20	20	27	22	29	20
Fe^{3+} no.	22	91	63	43	84	83	84	89	90	89	92	91	72	92

Sample:	Jor46.32	Jor46.26	Jor46.1	Jor46.21	Jor46.3	Jor46.19	Jor46.23	Jor46.28	Jor46.29	Jor46.30
P (MPa):	117	112	102	104	94	69	54	49	59	42
T (°C):	992	1010	1100	1020	1000	1000	975	1001	988	1010
SiO_2	0·11	0·11	0·08	0·29	0·31	0·08	0·10	0·14	0·35	0·09
TiO_2	6·27	6·96	3·35	5·30	6·20	5·89	3·00	5·22	12·55	4·96
Al_2O_3	4·00	4·49	4·45	3·68	1·26	5·23	3·51	5·01	4·09	4·97
Cr_2O_3	0·46	0·01	7·64	0·02	0·00	6·21	0·00	10·60	7·52	0·13
FeO	77·25	74·98	66·83	79·56	76·74	69·19	78·61	64·72	63·98	75·33
MnO	0·30	0·26	0·22	0·58	0·20	0·24	0·49	0·30	0·39	0·37
MgO	5·95	5·98	7·70	2·45	2·80	6·58	5·70	7·01	4·78	6·97
NiO	—	—	0·68	—	0·05	—	—	—	—	—
V_2O_3	0·26	0·18	—	0·32	—	0·17	—	0·02	0·36	0·05
Total	94·98	93·36	90·94	92·54	87·56	93·578	91·61	93·026	94·022	93·07
Fe_2O_3	54·43	51·77	50·73	53·01	51·27	47·58	60·26	43·93	31·77	55·87
FeO	28·27	28·40	21·18	31·87	30·60	26·38	24·39	25·19	35·89	25·05
Total	100·05	98·15	96·02	97·51	92·70	98·85	97·57	97·49	97·21	98·47
Cr no.	7	00	53	0	0	44	0	59	55	2
Mg no.	27	27	39	12	14	31	29	33	19	33
Fe^{3+} no.	89	88	77	90	96	76	92	70	69	88

*Representative analyses of natural spinel compositions (Luhr & Carmichael 1985): (a) spinel included in olivine; (b) representative groundmass composition.

NNO + ~2 (Table 1). Olivine is the liquidus phase at 10^5 Pa (Table 4), but our apparatus is unable to reach liquidus temperatures below 300 MPa, and thus the liquidus is poorly known. Olivine is followed in succession by spinel, apatite and augite at 200 MPa, and varies slightly in composition ($Fo_{89–86}$) above the hornblende stability field, but becomes more Fa rich at lower temperatures. The temperatures at which spinel, augite and apatite crystallize are separated by only a few tens of degrees. Hornblende without biotite occurs

Table 9: Experimental and natural clinopyroxene compositions

Sample:	Jor46[1]	Jor46[1]	MAS 2003a	Jor46.20	Jor46.10	Jor46.5	Jor46.8	Jor46.9	Jor46.24	Jor46.31	Jor46.32
P (MPa):	core	rim		232	221	199	214	154	126	121	117
T (°C):				1060	1035	1050	1035	1025	1040	967	992
n:			6	8	4	14	5	5	8	8	8
SiO_2	52·45	51·07	53·19	51·2(1·1)	51·40(1·3)	50·7(1·2)	51·6(1·9)	50·8(0·6)	49·8(1·1)	51·7(1·1)	50·8(1·0)
TiO_2	0·53	0·86	0·45	0·86(27)	0·7(4)	0·85(19)	0·9(4)	0·86(13)	1·13(28)	0·68(18)	0·90(25)
Al_2O_3	2·04	2·44	1·53	2·5(9)	2·7(1·0)	2·7(0·7)	2·6(1·1)	2·9(3)	3·3(8)	2·2(7)	2·7(7)
FeO*	4·71	6·50	4·95	5·9(9)	6·0(1·0)	5·8(5)	6·3(0·9)	6·7(0·9)	7·0(6)	5·4(9)	6·4(5)
MnO	0·08	0·11	0·09	0·12(2)	0·08(2)	0·12(2)	0·11(4)	0·15(6)	0·15(6)	0·13(4)	0·14(3)
MgO	16·01	15·11	16·75	15·5(7)	15·6(1·0)	15·8(6)	15·4(1·1)	15·4(4)	14·9(7)	16·1(7)	15·4(4)
CaO	23·02	22·62	22·63	22·29(23)	22·34(22)	22·1(4)	22·00(28)	22·01(41)	22·1(3)	22·10(26)	22·24(28)
Na_2O	0·42	0·45	0·41	0·46(9)	0·47(7)	0·38(6)	0·47(8)	0·49(6)	0·55(10)	0·47(8)	0·46(7)
Total	100·07	99·32	100·00	99·04	99·61	98·54	99·55	99·47	99·09	99·33	99·13
Wo	47·0	46·5	45·4	45·9	45·9	45·4	45·7	45·3	45·8	45·4	45·7
En	45·5	43·1	46·8	44·5	44·5	45·1	44·0	44·0	42·9	46·0	44·0
Fs	7·5	10·4	7·8	9·5	9·6	9·4	10·9	10·7	11·4	8·7	10·3

Sample:	Jor46.26	Jor46.25	Jor46.1	Jor46.21	Jor46.3	Jor46.19	Jor46.29	Jor46.23	Jor46.28	Jor46.22	Jor46.30
P (MPa):	112	110	102	104	94	69	59	54	49	48	42
T (°C):	1010	1010	1100	1020	1000	100	988	975	1001	950	1010
n:	5	7	5	8	3	8	6	8	6	5	7
SiO_2	51·2(8)	51·7(8)	49·9(1·5)	50·5(1·2)	50·9(1·8)	51·4(0·8)	51·3(1·0)	50·3(1·8)	52·0(7)	51·0(1·0)	51·5(8)
TiO_2	0·81(27)	0·69(18)	1·02(17)	0·9(3)	1·0(0·4)	0·86(25)	0·79(23)	1·1(5)	0·65(16)	0·81(19)	0·80(27)
Al_2O_3	2·4(8)	2·2(6)	3·3(9)	2·7(8)	2·6(1·2)	3·0(8)	2·4(7)	3·4(1·3)	2·0(6)	2·6(6)	2·1(7)
FeO*	6·5(4)	5·6(6)	6·3(6)	6·5(9)	6·2(1·6)	6·9(5)	6·4(7)	6·8(1·0)	5·5(6)	6·2(6)	6·2(8)
MnO	0·09(5)	0·10(3)	0·10(3)	0·13(5)	0·11(6)	0·1(3)	0·13(2)	0·17(5)	0·09(3)	0·12(3)	0·12(4)
MgO	15·6(5)	16·0(7)	15·2(5)	15·4(7)	16·0(9)	15·2(7)	15·7(6)	14·8(9)	16·0(4)	15·4(5)	15·9(5)
CaO	22·3(3)	22·5(5)	22·60(9)	22·2(4)	22·3(7)	22·4(5)	22·3(4)	21·9(6)	22·44(13)	22·7(3)	22·3(4)
Na_2O	0·41(4)	0·45(6)	0·46(4)	0·52(10)	0·41(7)	0·51(8)	0·42(8)	0·56(9)	0·39(6)	0·48(6)	0·41(9)
Total	99·42	99·63	99·394)	99·15	99·56	100·39	99·52	99·20	99·57	99·53	99·52
Wo	45·5	45·8	46·42	45·6	45·1	45·8	45·5	45·9	45·9	46·4	45·3
En	44·1	45·2	43·5	44·0	45·1	43·1	44·4	43·0	45·5	43·7	44·9
Fs	10·3	8·9	10.	10·4	9·8	11·1	10·3	11·2	8·7	9·9	9·8

[1] Analyses taken from Luhr & Carmichael (1985).
n, number of analyses; FeO*, total iron as FeO.

only over a very small temperature interval (Fig. 1), and is joined by biotite at higher pressures. Plagioclase ($An_{43–34}$) (Table 10) is stable at $P_{H_2O} < 75$ MPa for $T > 970$°C in the absence of biotite (Fig. 1).

Exploratory experiments at f_{O_2} values equivalent to NNO + 0·5 (Table 3) were performed to establish the effect of reducing f_{O_2} on the Cerro la Pilita magma (Fig. 2). It can be seen in Fig. 2 that the upper limit of hornblende stability is ~990°C, substantially less than its stability limit (~1040°C) in experiments at NNO + 2; olivine compositions are richer in the Fa component at the lower f_{O_2}. Curiously, hornblende without biotite is stable to 200 MPa at NNO + 0·5 whereas it is stable only to 150 MPa at NNO + 2 (Fig. 1). Amphibole compositions are more Fe rich (Table 8), but otherwise similar to those found in the more oxidizing experimental runs.

Water-undersaturated phase equilibria

Although solid–liquid experiments with a pure water fluid phase are simple to execute, it seems likely that

Table 10: Natural and experimental plagioclase compositions

Sample:	Jor46*	Jor46*	Jor46.22	Jor46.23	Jor46.30	Jor46.29
P (MPa):		—	48	54	42	59
T (°C):		—	1000	975	1010	988
n:	core	rim	4	11	1	2
SiO_2	55·46	55·61	55·14(55)	55·73(69)	56·34	56·32
Al_2O_3	26·00	26·25	26·40(24)	25·67(62)	23·20	22·82
FeO	0·96	1·09	0·95(12)	1·06(11)	1·75	0·97
CaO	8·08	8·18	8·60(23)	7·96(60)	6·81	7·25
Na_2O	5·83	5·72	5·79(10)	6·20(32)	6·39	6·27
K_2O	0·84	0·73	0·63(6)	0·73(14)	1·18	1·87
SrO	1·70	1·70	1·22	1·41(10)	1·20	1·12
BaO	0·47	0·35	0·14	0·25(9)	0·37	0·39
Total	99·34	99·63	97·91	99·63	98·60	97·60
Wt % An	40·1	40·6	42·7	39·5	33·8	36·0
Ab	49·3	48·4	49·0	52·5	54·1	53·1
Or + Sr	10·3	9·6	7·5	8·7	10·8	14·5

*Natural composition taken from Luhr & Carmichael (1985). *n*, number of analyses.

magmas may have other volatile components dissolved in the liquid, and both CO_2 and S are plausible additions. We found no petrographic evidence for a mineral containing S in the trachybasalt scoria; accordingly, we diluted the water component of the vapour phase by using oxalic acid, which gives a fluid composition of equal amounts of H_2O and CO_2 (Holloway & Wood, 1988). The results of three experiments are given in Table 2 and plotted in Fig. 3. Reducing the activity of water in the fluid phase results in the stabilization of plagioclase to higher pressures (>150 MPa) than in the water-saturated experimental runs, but the composition of the plagioclase remained about the same (Fig. 3), and not very different from the phenocryst composition (An_{40}; Table 10).

Comparison with the natural assemblage

A comparison of the experimentally determined phase equilibria with the petrological and textural features of the scoria can be used to constrain the conditions of storage of the magma. Hornblende forms euhedral phenocrysts and microphenocrysts in the scoria sample with oxidation rims absent or minute, whereas in the lava flow, hornblende is replaced by opacite almost completely. Experimental hornblendes exhibit some compositional variation as a function of pressure and temperature (Table 7) and those generated at P_{H_2O} of 100–130 MPa and temperatures between 1000 and 1020°C correspond most closely to those found in the phenocryst assemblage. One of the small differences between the natural and experimental results is K_2O, which in the hornblende of the scoria is 0·26%, but in both the experiments and the ejected blocks (MAS 2003*a*), it is higher (~1·1%) (Table 7). Hornblende compositions are more Fe rich in the lower f_{O_2} experiments, suggesting that the natural assemblage crystallized under the more oxidizing conditions similar to NNO + 2.

The average composition of olivine at temperatures above the onset of hornblende crystallization is Fo_{87} (Fig. 1), which corresponds within error (±1% Fo) to the composition of the most magnesian olivine cores in the Cerro la Pilita scoria ($Fo_{88–85}$; Luhr & Carmichael, 1985). CO_2 may have been only a minor component of the vapour phase, as the phenocrystic olivines compare well with those of water-saturated liquids (Fig. 1), rather than with those where CO_2 is equal to H_2O in the vapour phase (Table 2). Cr_2O_3-rich spinel (~40%) occurs as inclusions in the cores of the olivine phenocrysts (Table 8) but such Cr-rich compositions have not been reproduced within the *P*–*T* field of the experiments, although spinel with less Cr_2O_3 (26–16%) is found at the highest *P* and *T* (Table 8). Otherwise all the experimental spinel approaches the titanomagnetite of the groundmass in composition.

Little systematic compositional variation is found among the experimental augites, which have the general composition $Wo_{45·5}En_{44·5}Fs_{10}$ (Table 9). The augite phenocrysts of the scoria are zoned from $Wo_{47}En_{45·5}Fs_{7·5}$ cores to $Wo_{46·5}En_{43·1}Fs_{10·4}$ rims (Table 9, Luhr & Carmichael, 1985), whereas those from the biotite-bearing ejected blocks are more Mg rich ($Wo_{45·4}En_{46·8}Fs_{7·8}$). The experimental augites most closely resemble the phenocryst rim compositions, suggesting that the magma may have initially crystallized at higher pressures than those explored experimentally.

Although biotite is absent in the scoria, it is present in the ejected blocks (MAS 2003a), and its composition is generally similar to those of the experimental biotites (Table 11), except that Na_2O is higher, and K_2O lower in the experimental phases; the Mg number of biotite is higher than in the coexisting experimental olivine, a characteristic feature of lavas with olivine and biotite phenocrysts (Carmichael *et al.*, 1996). In our experiments, plagioclase feldspar that is compositionally similar to the high-Sr plagioclase microphenocrysts (~An_{40}, Table 10) is not stable in the presence of hornblende until P_{H_2O} is <60 MPa (~3 wt % H_2O) and the temperature is <1000°C (Fig. 1). We have interpreted the small size of the plagioclase microphenocrysts in the scoria, in contrast to the much larger and equant plagioclase phenocrysts in the ejected

Table 11: Natural and experimental biotite compositions

Sample:	MAS 2003a	Jor46.4	Jor46.10	Jor46.8	Jor46.7	Jor46.9	Jor46.31	Jor46.22
P (MPa):		223	221	214	207	154	121	48
T (°C):		1000	1035	1035	1025	1025	967	950
n:	6	3	4	1	8	5	1	5
SiO_2	38·43	37·5(4)	37·2(5)	37·26	37·6(5)	38·3(1·4)	39·19	35·70(45)
TiO_2	2·35	2·54(23)	3·46(27)	3·07	2·43(28)	3·1(4)	2·91	5·4(5)
Al_2O_3	14·88	14·30(3)	14·55(24)	14·04	15·6(1·0)	14·79(24)	14·76	14·95(19)
FeO	5·95	6·37(6)	8·58(20)	9·16	8·38(16)	9·1(6)	9·13	8·02(23)
MnO	0·04	0·07(2)	0·06(1)	0·09	0·05(3)	0·05(3)	0·09	0·04(2)
MgO	21·63	22·38(23)	20·02(23)	19·37	20·7(5)	18·1(1·5)	17·92	18·0(6)
CaO	0·06	0·07(1)	0·08(3)	0·11	0·07(6)	0·27	0·25	0·83
Na_2O	0·77	1·25(1)	1·21(4)	1·29	1·45(16)	1·38(15)	1·29	1·39(2)
K_2O	9·10	7·97(8)	8·15(12)	8·09	8·05(14)	7·7(7)	7·35	7·56(13)
Total	95·68*	92·44	94·60	93·07	95·39	94·06	94·06	91·84
BaO	0·46					0·82(14)	0·74	
F	1·15					0·36(5)	0·32	
Fe_2O_3†		3·78	3·34	—	—	—	4·97	—
FeO		2·97	5·57	—	—	—	4·66	—
Mg no.		93	86	—	—	—	87	—

*Includes 0·84 Cr_2O_3.
†Ratio of Fe_2O_3 to FeO calculated using calculated ratio in glass.

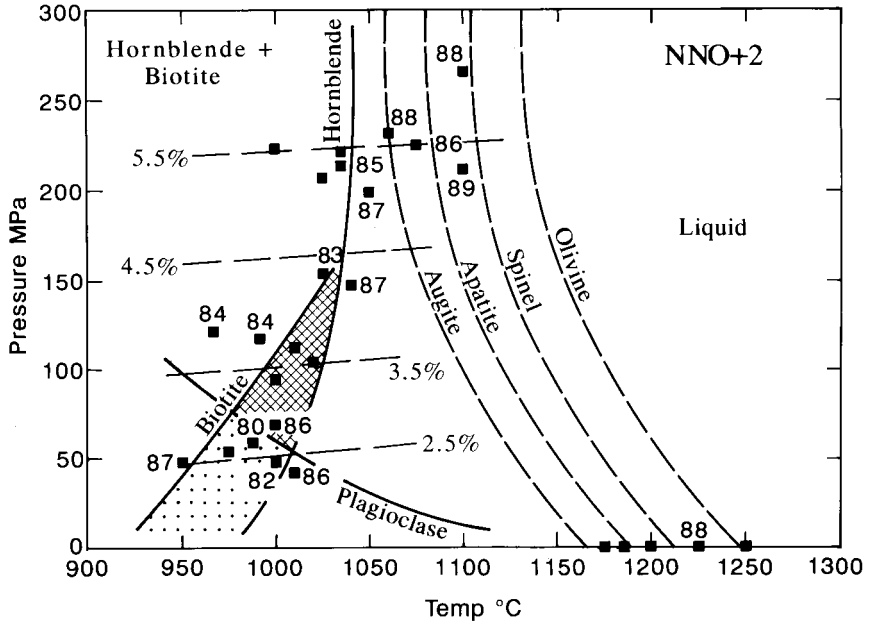

Fig. 1. Phase stability felds of trachybasalt (Tables 1 and 4) at NNO + ~2; ■, water-saturated liquid composition. Boundary curves are continuous lines, and are labelled for the phases that crystallize on the low-temperature side. Dashed lines are water isopleths (wt %) calculated from Moore *et al.* (1998). Numbers by runs refer to the Fo content of the olivine (Table 6). Cross-hatched area represents the phenocryst (ol + pyx + ap + hb + spinel) equilibration *P*–*T* region, without plagioclase. The plagioclase stability region is below the cross-hatched area.

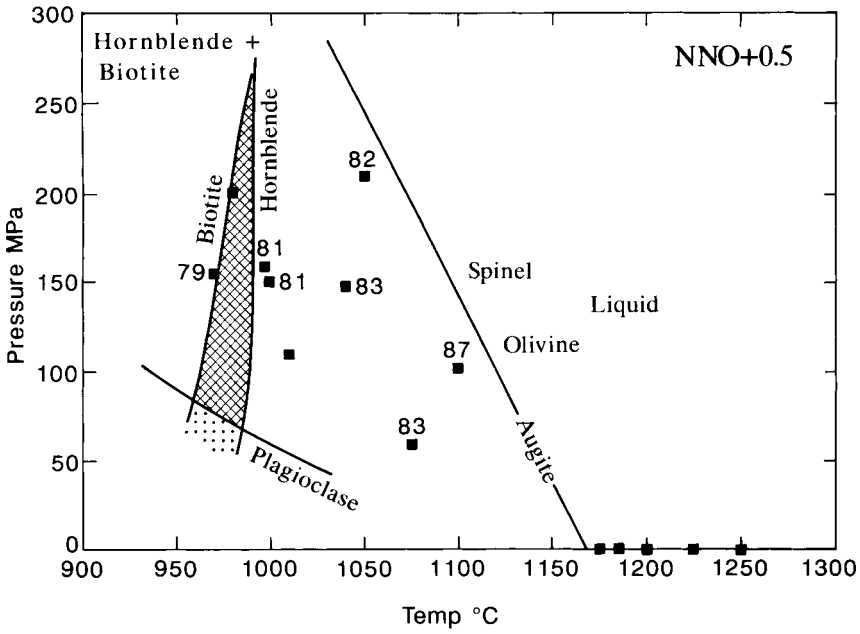

Fig. 2. Phase stability fields for water-saturated liquids at NNO + 0·5 (Table 3), with numbers representing the Fo content of olivine (Table 3). Cross-hatched area is P–T region of equilibration of phenocryst assemblage (ol, ap, pyx, hb, spinel).

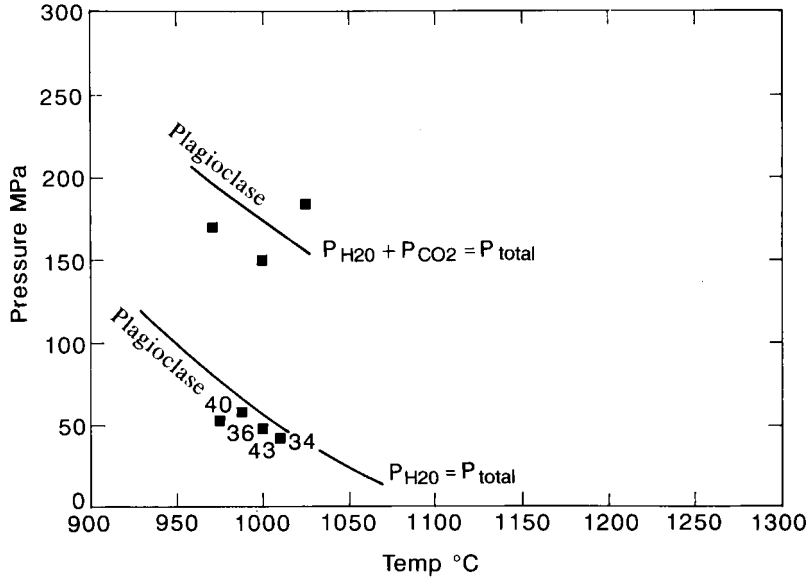

Fig. 3. Composition of plagioclase in runs with $P_{H_2O} = P_{CO_2}$ (Table 2) showing the inferred upper stability boundaries for plagioclase. Lower curve is taken from Fig. 1 and Table 10.

blocks (MAS 2003a), as resulting from decompressional crystallization on ascent, rather than as equilibration in the plagioclase stability field.

The absence of biotite in the natural phenocryst assemblage of Jor 46 constrains the phenocryst equilibration of the magma to P_{H_2O} <150 MPa, and to water concentrations of <4·5 wt % (Fig. 1). Both hornblende and biotite reach a temperature maximum of ~1040°C at pressures of 200 MPa, but our experiments cannot separate their stability limits above 170 MPa. Consequently, there is a limited range of P–T conditions (<1000°C, <70 MPa) at which plagioclase and hornblende, without biotite, are capable of coexisting in this water-saturated trachybasalt liquid at NNO + ~2. The presence of both biotite and plagioclase in a limited number of the eruptive products from

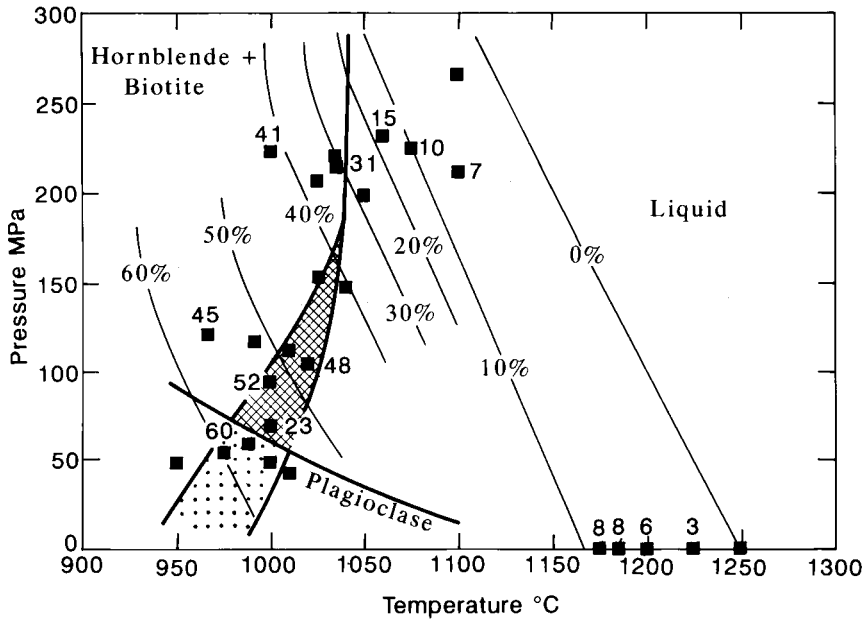

Fig. 4. Contours of crystallinity (wt %) taken from Table 5 and Fig. 1, with numbers beside runs representing the calculated percentage. The anomalous position of the liquid with 23% crystals should be noted.

Cerro la Pilita suggests that some of the magma passed through P–T conditions on or close to these phase boundaries during ascent. It is also worth noting that hornblende crystallization would be suppressed to significantly lower temperatures at lower f_{O_2} values, reducing the P–T interval where hornblende could crystallize in the absence of plagioclase.

Crystallinity and liquid compositions

For each of the experimental runs that has an analysed glass composition (Table 5), the mode of that run has been calculated as described above, and the total amount of crystals (the crystallinity) ± 10% is given in Table 5. In Fig. 4, contours of crystallinity have been drawn using the values of Table 4, but the contours are not well constrained. However, their general form is correct, and show that with falling temperature and pressure, there is an increase in crystallinity; this same feature is found in the crystallinity curves of an andesite composition (Blatter & Carmichael, 2001).

The experimental glass compositions (Table 5) are *ne*-normative at higher temperatures, becoming successively *hy*-normative with some of the most evolved liquids becoming *q*-normative at lower temperatures. This is a consequence of the precipitation of hornblende, which is very silica poor (Table 8) in contrast to the bulk composition of the lava (Table 5). These siliceous liquids are equivalent to high-K dacites according to the classifications of LeMaitre *et al.* (1989) and Gill (1981), respectively. Because the highest pressures of our water-saturated experiments were only ~200 MPa, the compositions of these liquids will not be representative of liquids generated by partial melting of a crystalline trachybasalt (saturated or undersaturated with water) at the base of the crust (>1 GPa), nor are the melt fractions (>40%) small enough to represent the compositional trend of small to moderate degrees of melting of underplated trachybasalt. Nevertheless, it is evident that *q*-normative liquids can be generated by partial fusion of an *ne*-normative basalt.

DISCUSSION

The Cerro la Pilita trachybasalt: intensive variables and the ascent path from the mantle

Comparison of the natural and experimental assemblage has provided several very important constraints on the depth of crystallization of the Cerro la Pilita magma. The absence of biotite in the Cerro la Pilita basaltic scoria provides a constraint on the depth of crystallization of the scoria phenocryst assemblage (Fig. 1). The phenocryst assemblage of hornblende, augite, apatite and olivine equilibrated between 1040°C and 970°C, with water contents between 4·5 and 2·5 wt % (Fig. 1). A combination of zoning in the augite phenocrysts, and Cr-rich spinel inclusions in the olivine, indicates that the trachybasalt magma was initially hotter than the phenocryst equilibration region of Fig. 1. The presence of biotite and plagioclase

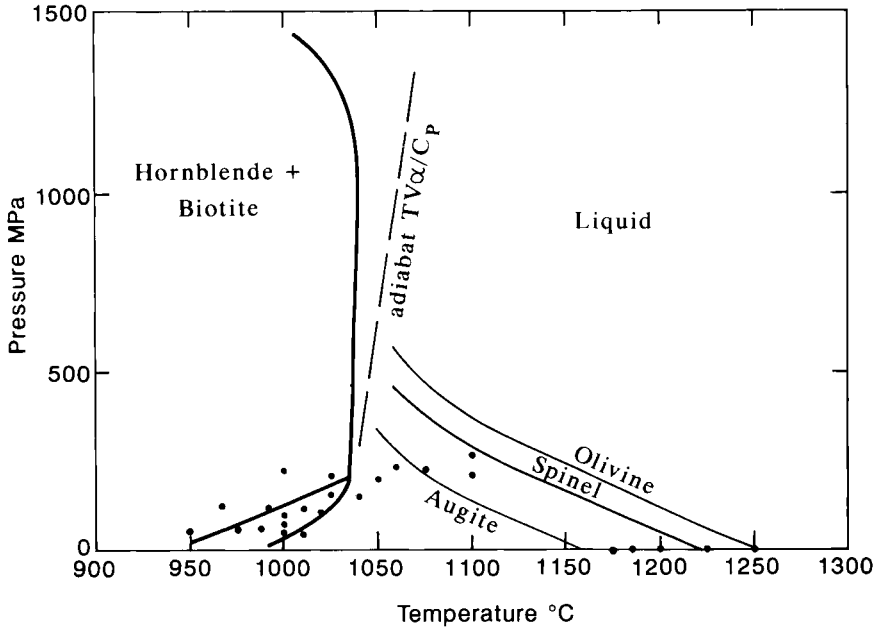

Fig. 5. Boundary curves of Fig. 1 extrapolated to higher pressures, based on the experimental results of Allen & Boettcher (1983) and Holloway & Burnham (1972) for hornblende, which is assumed to have the same stability as biotite. The calculated adiabat assumes 6 wt % H_2O, and uses the data of Lange & Carmichael (1990), Ochs & Lange (1999) and Spera (2000) for the trachybasalt Jor 46 (Luhr & Carmichael, 1985).

in the ejected blocks suggests that some portions of the magma equilibrated at greater depths and/or experienced partial degassing at some point prior to eruption.

In Fig. 5, the temperature of the trachybasalt magma has been extrapolated from the phenocryst equilibration stage to the base of the crust (1·0 GPa), using a calculated adiabat ($TV\alpha/C_p$) that varies from $2{\cdot}7^\circ/10^8$ Pa for an anhydrous magma to $4{\cdot}7^\circ/10^8$ Pa for one containing 6% water. It can be seen (Fig. 5) that olivine may have precipitated in the ascending magma at about 600 MPa (~18 km) followed by augite at lower pressures before the magma entered the hornblende stability field. An ascending magma appears far more likely to enter the biotite + hornblende field than it is to intersect the hornblende-only field, although only ejected blocks with biotite + hornblende have been found, whereas both scoria and a 2 km long lava flow lack biotite. A hydrous magma missing the stability fields of biotite + hornblende or hornblende would have phenocrysts of olivine, Cr-spinel and augite, and could suppress plagioclase, which is the characteristic phenocryst assemblage of the absarokites in western Mexico (Carmichael *et al.*, 1996).

The role of hornblende crystallization in prohibiting magma eruption

The analysis of sample crystallinities also affords the opportunity to assess physical changes in the magma state during ascent and eruption. From Marsh's (1981) Aleutian modal data, magmas with more than 50–55% crystals are not found as lavas, presumably because their viscosity is too high to allow upward flow in the conduit. This limit reflects a change in the rheological regime, whereby magma behaves more like a brittle solid rather than a ductile mass, which occurs as a result of high crystal concentration within the magma. The experiments of LeJeune & Richet (1995) on a simple silicate liquid identified an abrupt change of rheology at crystal concentration of ~40 vol. %, where clustered crystals start to strongly oppose shear deformation. In most silicate magmas the limit of crystal concentration beyond which magmas have an 'infinite' viscosity is assumed to be ~60 vol. %, the value for a monodisperse suspension (Pinkerton & Stevenson, 1992). Thus for crystal concentrations of between 40 and 60 vol. %, eruption of a magma body becomes highly unlikely; the imposition of a pressure gradient across the body is more likely to result in the migration and percolation of any remaining melt via brittle cracks rather than ductile migration of the entire body (Bagdassarov & Dorfman, 1998).

It would therefore seem that an eruptible limit of ~ 50% crystallinity would preclude trachybasalt magmas that had entered the plagioclase field (see Fig. 4) from erupting, and that unless the presence of CO_2 shifts the plagioclase field to higher pressures (Fig. 3), and hence to lower crystallinities, plagioclase-bearing

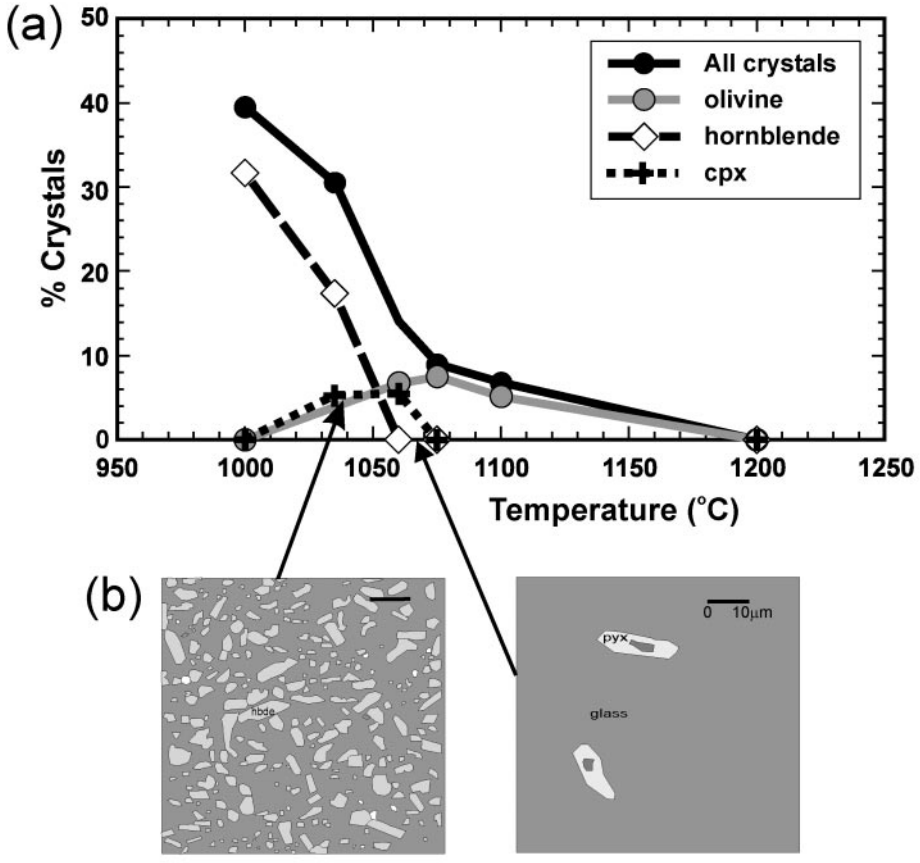

Fig. 6. (a) Calculated modal amounts (wt %) of olivine, augite and hornblende (Table 5) at ~200 MPa showing the increase of crystallinity with isobaric cooling, and the decrease in olivine and augite as hornblende increases in abundance. (b) Sketch overlays of scanning electron micrographs to show the abundance and morphology of crystals above and below the onset of hornblende crystallization. Scale bars represent 10 μm.

lavas with phenocrysts of hornblende, augite, apatite and olivine will not occur. However, there is one anomalous value of crystallinity in Fig. 4 (23 wt %) that is inconsistent with the pattern of crystallinities, and it is close to the value of the natural assemblage (~20 vol. %); perhaps there is indeed an anomalous region of low crystallinity, but the evidence to support this is weak.

Holloway & Burnham (1972), in a study on the melting relations of a Kilauea tholeiite, first recognized the large increase in the amount of liquid as the hornblende breakdown temperature was exceeded. Looked at from the perspective of magma cooling, there will be a large increase in crystallinity at the onset of hornblende precipitation, and Holloway & Burnham illustrated this with two isobaric sections. In Fig. 6, we have plotted the crystallinity of the trachybasalt at ~200 MPa (Fig. 1; Table 5) which clearly shows this marked increase in crystallinity, and also the decrease in olivine and augite accompanying the precipitation of hornblende; this is a reaction relationship that has also been recognized by Helz (1973), Grove *et al*. (1997) and Moore & Carmichael (1998).

In Fig. 7, the increase of crystallinity accompanying the isobaric crystallization of hornblende in hydrous basaltic, basaltic andesite and andesitic liquids is plotted for a group of experiments taken from the literature. As a larger proportion of the components of basalt can be taken up in hornblende (regardless of the exact composition of the basalt and hornblende), in comparison with andesite, the increase of crystallinity is larger in basalts than in andesites (Fig. 7). It is postulated that the paucity of subduction-related trachybasalts, or basaltic magmas, at the Earth's surface may not be a consequence of their absence within the suprasubduction-zone lithosphere, but rather a result of the onset of high crystallinities with the precipitation of hornblende near the base of the crust.

On leaving the upper mantle, an ascending hydrous magma will intersect a cooler crust, but rather than crystallize by decompression as it does on nearing the surface, it will be trapped and crystallize isobarically.

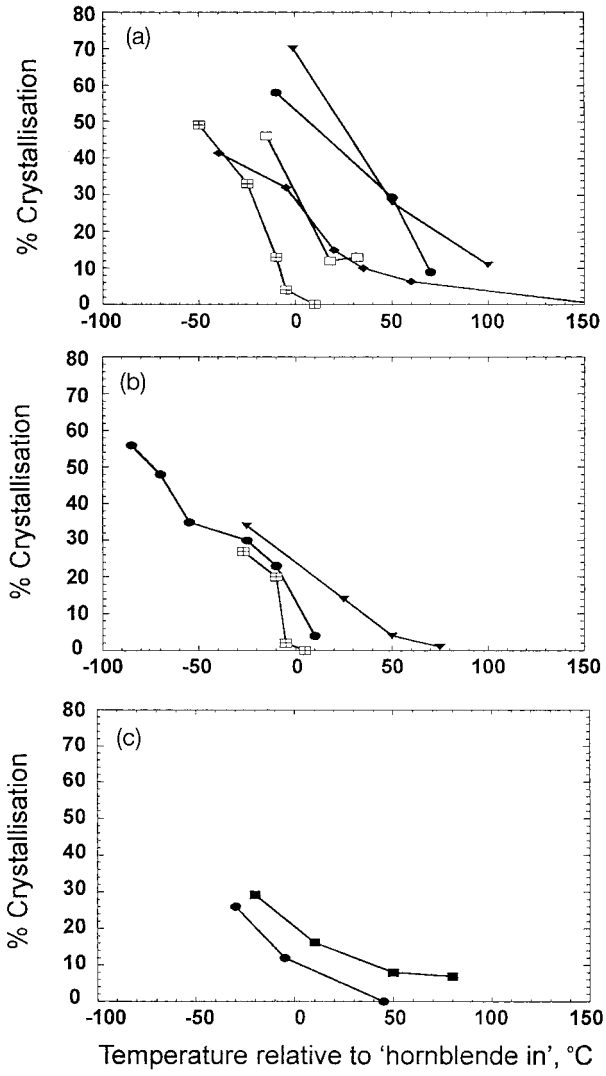

Fig. 7. Total phenocryst content as a function of temperature at P_{H_2O}=200 MPa (calculated relative to hornblende-in temperature for each composition). (a) Basalts (<52 wt % SiO_2): ■ and square with cross, high-alumina basalts from Sisson & Grove (1993); diamonds, Jor46 this study; ●, Foden & Green (1992); ▼, alkali basalt, Holloway & Burnham (1972). (b) Basaltic andesites (52–59 wt % SiO_2): squares with cross, Sisson & Grove (1993); ●, Grove *et al.* (1997); ▼, Moore & Carmichael (1998). (c) Andesites (>59 wt % SiO_2): ■, Blatter & Carmichael (1998); ●, Moore & Carmichael (1998).

Under these conditions the crystallinity curves depicted in Fig. 7 will influence the magma's capacity to flow, and once hornblende crystallizes, the magma's ascent is retarded by its high crystallinity. Successive hydrous basaltic magmas will become stock-piled at the base of the crust. This effect is more evident in basaltic magmas than in andesitic magmas because a greater proportion of the basaltic bulk composition can crystallize as hornblende than it can for andesite. Thus in more evolved melts the crystallization of hornblende increases the viscosity less, and the significant barrier to magma ascent and eruption is reduced.

Basaltic stock-piling

If hornblende crystallization were to effectively freeze and stall wet basaltic melts within or at the base of the crust then geological evidence for this process should be found within some subduction-related magmas. This should include: (1) hornblende-rich gabbros in exhumed subduction zones; (2) the presence of hornblende-rich mafic xenoliths or inclusions within more evolved volcanic suites or plutons; (3) petrological and geochemical evidence for the role of residual hornblende after subsequent remobilization, reheating and differentiation of these accumulated melts; (4) a paucity of hornblende-bearing basalts erupted as scoria and lava. The relative scarcity of erupted hornblende-bearing basalts has been described earlier, and Arculus & Wills (1980) contrasted this with the relative abundance of hornblende-bearing mafic xenoliths in island-arc settings. In the case of Cerro la Pilita we suggest that eruption occurred as a consequence of comparatively small degrees of undercooling within the hornblende stability field (as evidenced by the continued presence of augite).

Hornblende-bearing gabbros are a relatively common feature of exhumed subduction zones and in examples of the mafic lower crust [e.g. Onion Sill Gabbro, California, Sisson *et al.* (1996); Kamchatka, Russia, Kepezhinskas *et al.* (1993); the Coastal Batholith, Peru, Mason (1985); Adamello Massif, Italy, Ulmer *et al.* (1983), Blundy & Sparks (1992); lower-crustal examples from Rudnick & Fountain (1995)]. Modal proportions of hornblende can be as much as 50 vol. % of the rock and hornblende commonly forms as a reaction product around earlier formed clinopyroxene phenocrysts in an analogue to the reaction observed in our equilibrium experiments.

Additionally, the accumulation and subsequent remelting of hornblende-rich basaltic magmas within the lower crust has also been invoked to explain geochemical variations in some calc-alkaline volcanic suites and plutons [e.g. Lassen, California, Borg & Clynne (1998); North Cascades, Tepper *et al.* (1993); Aurora Volcanic Field, Lange & Carmichael (1996); central Aleutians, Alaska, Romick *et al.* (1992)].

Thus basaltic stock-piling does indeed occur in the lower crust and this mechanism in turn supports the concept that rapid hornblende crystallization at any point during the ascent of a hydrous basaltic melt would reduce the magma's eruptibility. Subsequent remelting and remobilization can generate a wide variety of melt compositions and these processes should

thus be taken into account in models of subduction-zone magmatism.

ACKNOWLEDGEMENTS

We would like to thank James Brophy and Richard Arculus for careful and useful reviews. The first author would like to thank Dawnika Blatter for assistance and advice in the laboratory and beyond, and John Donovan is thanked for his advice on the use of the electron microprobe. In another context Jim Brophy offered some elegant ideas on representing crystallinity, and Ethan Baxter provided some essential probe analyses at the last minute. To all the second author is indebted. The support of NSF EAR 97-06129 was essential to the research.

REFERENCES

Allen, J. C. & Boettcher, A. L. (1983). The stability of amphibole in andesite and basalt at high pressure. *American Mineralogist* **68**, 307–314.

Anderson, A. T. (1974). Chlorine, sulfur and water in magmas and oceans. *Geological Society of America Bulletin* **85**, 1485–1492.

Anderson, A. T. (1979). Water in some hypersthenic magmas. *Journal of Geology* **87**, 509–531.

Arculus, R. J. & Wills, M. J. (1980). The petrology of plutonic blocks and inclusions from the Lesser Antilles Island Arc. *Journal of Petrology* **21**, 743–799.

Arculus, R. J., Delong, S. E., Kay, R. W., Brooks, C. & Sun, S. S. (1977). The alkalic rock suite of Bogoslof Island, Eastern Aleutian Arc, Alaska. *Journal of Geology* **85**, 177–186.

Arculus, R. J., Johnson, R. W., Chappell, B. W., McKee, C. O. & Sakai, H. (1983). Ophiolite-contaminated andesites, trachybasalts and cognate inclusions of Mount Lamington, Papua New Guinea: anhydrite–amphibole-bearing lavas and the 1951 cumulodome. *Journal of Volcanology and Geothermal Research* **18**, 215–258.

Bagdassarov, N. & Dorfman, A. (1998). Granite rheology: magma flow and melt migration. *Journal of the Geological Society, London* **155**, 863–872.

Barton, M. & Wyers, G. P. (1991). Estimates of P, T, PH_2O and f_{O_2} for lavas from Patmos (Greece) and implications for magmatic evolution. *Journal of Volcanology and Geothermal Research* **47**, 265–297.

Blatter, D. L. & Carmichael, I. S. E. (1998). Plagioclase-free andesites from Zitacuaro (Michoacan), Mexico: petrology and experimental constraints. *Contributions to Mineralogy and Petrology* **132**, 121–138.

Blatter, D. L. & Carmichael, I. S. E. (2001). Hydrous phase equilibria of a Mexican high-silica andesite: a candidate for mantle origin? *Geochimica et Cosmochimica Acta* **65**, 4043–4065.

Blundy, J. D. & Sparks, R. S. J. (1992). Petrogenesis of mafic inclusions in granitoids of the Adamello Massif, Italy. *Journal of Petrology* **33,** 1039–1104.

Borg, L. E. & Clynne, M. A. (1998). The petrogenesis of felsic calc-alkaline magmas from the southernmost Cascades, California: origin by partial melting of basaltic lower crust. *Journal of Petrology* **39**, 1197–1222.

Bower, S. M. & Woods, A. W. (1997). Control of magma volatile content and chamber depth on the mass erupted during explosive volcanic eruptions. *Journal of Geophysical Research* **102**, 10273–10290.

Brown, F. H. & Carmichael, I. S. E. (1969). Quaternary volcanoes of the Lake Rudolf region: 1. The basanite–tephrite series of the Korath range. *Lithos* **2**, 239–260.

Carmichael, I. S. E., Lange, R. A. & Luhr, J. F. (1996). Quaternary minettes and associated volcanic rocks of Mascota, western Mexico: a consequence of plate extension above a subduction modified mantle wedge. *Contributions to Mineralogy and Petrology* **124**, 302–333.

Deer, W. A., Howie, R. A. & Zussman, J. (1997). *Rock-forming Minerals. Vol 3: Sheet Silicates*. Harlow: Longman.

Donovan, J. J. & Tingle, T. N. (1996). An improved mean atomic number background correction for quantitative microanalysis. *Journal of the Microscopy Society of America* **2**, 1–7.

Foden, J. D. & Green, D. H. (1992). Possible role of amphibole in the origin of andesite: some experimental and natural evidence. *Contributions to Mineralogy and Petrology* **109**, 479–493.

Gaetani, G. A., Grove, T. L. & Bryan, W. B. (1993). The influence of water on the petrogenesis of subduction-related igneous rocks. *Nature* **365**, 332–334.

Gill, J. B. (1981). *Orogenic Andesites and Plate Tectonics*. Berlin: Springer.

Grove, T. L., Donnelly-Nolan, J. M. & Housh, T. (1997). Magmatic processes that generated the rhyolite of Glass Mountain, Medicine Lake Volcano, N. California. *Contributions to Mineralogy and Petrology* **127**, 205–223.

Helz, R. T. (1973). Phase relations of basalts in their melting range at $PH_2O = 5$ kb as a function of oxygen fugacity. Part I. Mafic phases. *Journal of Petrology* **14**, 249–302.

Holloway, J. R. & Burnham, C. W. (1972). Melting relations of basalt with equilibrium water pressure less than total pressure. *Journal of Petrology* **13**, 1–29.

Holloway, J. R. & Wood, B. J. (1988). *Simulating the Earth: Experimental Geochemistry*. London: Unwin Hyman.

Holloway, J. R., Dixon, J. E. & Pawley, A. R. (1992). An internally heated, rapid-quench, high-pressure vessel. *American Mineralogist* **77**, 643–646.

Hort, M. (1998). Abrupt change in magma liquidus temperature because of volatile loss or magma mixing; effects on nucleation, crystal growth and thermal history of the magma. *Journal of Petrology* **39**, 1063–1076.

Kawamoto, T. & Holloway, J. R. (1997). Melting temperature and partial melt chemistry of H_2O-saturated mantle peridotite to 11 Gigapascals. *Science* **240**, 240–243.

Kepezhinskas, P. K., Reuber, I., Tanaka, H. & Miyashita, S. (1993). Zoned calc-alkaline plutons in northeastern Kamchatka, Russia: implications for the crustal growth in magmatic arcs. *Contributions to Mineralogy and Petrology* **49**, 147–174.

Kress, V. C. & Carmichael, I. S. E. (1991). The compressibility of silicate liquids containing Fe_2O_3 and the effect of composition, temperature, oxygen fugacity and pressure on their redox states. *Contributions to Mineralogy and Petrology* **108**, 82–92.

Lange, R. A. & Carmichael, I. S. E. (1990). Thermodynamic properties of silicate liquids with emphasis on density, thermal expansion and compressibility. In: Nicholls, J. & Kelly, J. K. (eds) *Modern Methods of Igneous Petrology. Mineralogical Society of America, Reviews in Mineralogy* **24**, 25–64.

Lange, R. A. & Carmichael, I. S. E. (1996). The Aurora volcanic field, California–Nevada: oxygen fugacity constraints on the development of andesitic magma. *Contributions to Mineralogy and Petrology* **125**, 167–185.

Leake, B. E., Woolley, A. R., Arps, C. E. S. *et al.* (1997). Nomenclature of amphiboles: report of the subcommittee on amphiboles of the International Mineralogical Association, commission on new minerals and mineral names. *American Mineralogist* **82**, 1019–1037.

LeJeune, A.-M. & Richet, P. (1995). Rheology of crystal-bearing silicate melts: an experimental study at high viscosities. *Journal of Geophysical Research* **100**, 4215–4229.

LeMaitre, R. W., Bateman, P., Dudek, A., Keller, J., Lameyre, Le Bas, M. J., Sabine, P. A., Schmid, R., Sorensen, H., Streickesen, A., Woolley, A. R. & Zanettin, B. (1989). *A Classification of Igneous Rocks and Glossary of Terms*. Oxford: Blackwell.

Luhr, J. F. & Carmichael, I. S. E. (1981). The Cohima volcanic complex, Mexico, II The Late Quaternary cinder cones. *Contributions to Mineralogy and Petrology* **76**, 127–147.

Luhr, J. F. & Carmichael, I. S. E. (1985). Jorullo Volcano, Michocoan, Mexico (1759–1774): the earliest stages of fractionation in calc-alkaline magmas. *Contributions to Mineralogy and Petrology* **90**, 142–161.

Marsh, B. (1981). On the crystallinity, probability of occurrence and rheology of lava and magma. *Contributions to Mineralogy and Petrology* **78**, 85–91.

Mason, G. H. (1985). The mineralogy and textures of the Coastal Batholith, Peru. In: Pitcher, W. S., Atherton, M. P., Cobbing, E. J., *et al.* (eds) *Magmatism at a Plate Edge*. Glasgow: Blackie.

Moore, G. M. & Carmichael, I. S. E. (1998). The hydrous phase equilibria (to 3 kbar) of an andesite and basaltic andesite from Western Mexico: constraints on water content and conditions of phenocryst growth. *Contributions to Mineralogy and Petrology* **130**, 304–319.

Moore, G. M., Vennemann, T. & Carmichael, I. S. E. (1998). An empirical model for the solubility of H_2O in magmas to 3 kilobars. *American Mineralogist* **83**, 36–42.

Ochs, F. A. & Lange, R. A. (1999). Density of hydrous magmatic liquids. *Science* **287**, 1314–1317.

Pe-Piper, G. & Piper, D. (1992). Geochemical variation with time in the Cenozoic high-K volcanic rocks of the island of Lesbos, Greece; significance for shoshonite petrogenesis. *Journal of Volcanology and Geothermal Research* **53**, 371–387.

Pinkerton, H. & Stevenson, R. J. (1992). Methods of determining the rheological properties of magmas at sub-liquidus temperatures. *Journal of Volcanology and Geothermal Research* **53**, 47–66.

Pownceby, M. I. & O'Neill, H. S. C. (1994). Thermodynamic data from redox reactions at high temperatures III. Activity composition relations in Ni–Pd alloys from EMF measurements at 850–1250 K, and calibration of the NiO + Ni–Pd assemblage as redox sensor. *Contributions to Mineralogy and Petrology* **116**, 327–339.

Prouteau, G., Scaillet, B., Pichavant, M. & Maury, R. (2001). Evidence for mantle metasomatism by hydrous silicic melts derived from subducted oceanic crust. *Nature* **410**, 197–200.

Romick, J. D., Kay, S. M. & Kay, R. W. (1992). The influence of amphibole fractionation on the evolution of calc-alkaline andesite and dacite tephra from the central Aleutians, Alaska. *Contributions to Mineralogy and Petrology* **112**, 101–118.

Rudnick, R. L. & Fountain, D. M. (1995). Nature and composition of the continental crust: a lower crustal perspective. *Reviews of Geophysics* **33**, 267–309.

Rutherford, M. J., Sigurdsson, H., Carey, S. & Davis, A. (1985). The May 18, 1980, eruption of Mt. St. Helens 1. Melt composition and experimental phase equilibria. *Journal of Geophysical. Research* **90**, 2929–2947.

Ruxton, B. P. (1966). A late Pleistocene to recent rhyodacite–trachybasalt–basaltic latite volcanic association in Papua. *Journal of Geological Society of Australia* **13**, 41–56.

Sigurdsson, H. & Shepherd, J. B. (1974). Amphibole-bearing basalts from the submarine volcano Kick 'Em Jenny in the Lesser Antilles Island Arc. *Bulletin of Volcanology* **38**, 891–910.

Sisson, T. W. & Grove, T. L. (1993). Experimental investigations of the role of H_2O in calc-alkaline differentiation and subduction zone magmatism. *Contributions to Mineralogy and Petrology* **113**, 143–166.

Sisson, T. W. & Layne, G. D. (1993). Experimental investigations of the role of H_2O in calc-alkaline differentiation and subduction zone magmatism. *Contributions to Mineralogy and Petrology* **113**, 143–166.

Sisson, T. W., Grove, T. L. & Coleman, D. S. (1996). Hornblende gabbro sill complex at Onion Valley, California, and a mixing origin for the Sierra Nevada Batholith. *Contributions to Mineralogy and Petrology* **126**, 81–108.

Sparks, R. S. J., Barclay, J., Jaupart, C., Mader, H. M. & Phillips, J. C. (1994). Physical aspects of magmatic degassing I. Experimental and theoretical constraints on vesiculation. In: Carroll, M. R. & Holloway, J. R. (eds) *Volatiles in Magmas*. *Mineralogical Society of America, Reviews in Mineralogy* **30**, 413–443.

Spera, F. J. (2000). Physical properties of magmas. In: Sigurdsson, H. (ed.) *Encyclopaedia of Volcanoes*. London: Academic Press, pp. 171–191.

Stormer, J. C., Jr & Nicholls, J. (1981). XLFRAC; a program for the interactive testing of magmatic differentiation models. *Computers and Geosciences* **4,** 143–159.

Tepper, J. H., Nelson, B. K., Bergantz, G. W. & Irving, A. J. (1993). Petrology of the Chilliwack Batholith, North Cascades, Washington: generation of calc-alkaline granitoids by melting of mafic lower crust with variable water fugacity. *Contributions to Mineralogy and Petrology* **113**, 333–351.

Thomas, N. & Tait, S. R. (1997). The dimensions of magmatic inclusions as a constraint on the physical mechanism of mixing. *Journal of Geophysical Research* **75**, 167–178.

Ulmer, P., Callegari, E. & Sonderegger, U. C. (1983). Genesis of the mafic and ultramafic rocks and their genetical relations to the tonalitic–trondhjemitic granitoids of the southern part of the Adamello Batholith (Northern Italy). *Memorie della Società Geologica Italiana* **26**, 171–122.

Wallace, P. & Carmichael, I. S. E. (1992). Alkaline and calc-alkaline lavas near Los Volcanes, Jalisco, Mexico: geochemical diversity and its significance in volcanic arcs. *Contributions to Mineralogy and Petrology* **111**, 423–439.

Weber, C. & Pichavant, M. (1986). Plagioclase–liquid phase relations in the system Qz–Or–Ab–An–H_2O at 3 kbar: toward a resolution of experimental difficulties. *EOS Transactions, American Geophysical Union* **67**, 408.

Wyers, G. P. & Barton, M. (1986). Petrology and evolution of transitional alkaline-sub alkaline lavas from Patmos, Dodecanesos, Greece; evidence for fractional crystallization, magma mixing and assimilation. *Contributions to Mineralogy and Petrology* **93**, 297–311.